# A Tripartite Complex HIV-1 Tat-Cyclophilin A-Capsid Protein Enables Tat Encapsidation That Is Required for HIV-1 Infectivity

Malvina Schatz, Laetitia Marty, Camille Ounadjela, Phuoc Bao Viet Tong, Ilaria Cardace, Clément Mettling, Pierre-Emmanuel Milhiet, Luca Costa, Cédric Godefroy, Martine Pugnière, et al.

# A tripartite complex HIV-1 Tat-cyclophilin A-capsid protein enables Tat encapsidation that is required for HIV-1 infectivity

Malvina Schatz[1¶], Laetitia Marty[1¶], Camille Ounadjela [1¶], Phuoc Bao Viet Tong[1], Ilaria Cardace[1], Clément Mettling[2], Pierre-Emmanuel Milhiet[3], Luca Costa[3], Cédric Godefroy[3], Martine Pugnière[4], Jean-François Guichou[3], Jean-Michel Mesnard[1], Mickaël Blaise[1] and Bruno Beaumelle[1]*

[1]Institut de Recherche en Infectiologie de Montpellier, UMR 9004 CNRS, Université de Montpellier, 1919 Route de Mende, 34293 Montpellier, France
[2]Institut de Génétique Humaine, UPR 1142 CNRS, 141 Rue de la Cardonille, 34396 Montpellier, France
[3]Centre de Biologie Structurale, Université de Montpellier, CNRS, INSERM, 29 rue de Navacelles, 34090 Montpellier, France
[4]Institut de Recherche en Cancérologie de Montpellier, INSERM U 1194, 208 Rue des Apothicaires, 34298 Montpellier, France

[¶]These authors contributed equally to this work
*Corresponding author bruno.beaumelle@irim.cnrs.fr

**Running Title** An HIV-1 Tat encapsidation complex

**Abstract**

HIV-1 Tat is a key viral protein that stimulates several steps of viral gene expression. Tat is especially required for the transcription of viral genes but it is still not clear if and how Tat is incorporated into HIV-1 virions. Cyclophilin A (CypA) is a prolylisomerase that binds to HIV-1 capsid protein (CA) and is thereby encapsidated (200-250 copies of CypA /virion). Here we found that a Tat-CypA-CA tripartite complex assembles in HIV-1 infected cells and allows Tat encapsidation into HIV virions (1 Tat /1 CypA). Biochemical and biophysical studies showed that high-affinity interactions drive the assembly of the Tat-CypA-CA complex that could be purified by size-exclusion chromatography.
We prepared different types of viruses devoid of transcriptionally-active Tat. They showed a 5-10 fold decrease in HIV-infectivity and, conversely, encapsidating Tat into ΔTat viruses greatly enhanced infectivity. The absence of encapsidated Tat decreases the efficiency of reverse transcription by ~50% and transcription by more than 90%. We thus identified a Tat-CypA-CA complex that enables Tat encapsidation and showed that encapsidated Tat is required to initiate robust viral transcription and thus viral production at the beginning of cell infection, before neosynthesized Tat becomes available.

**Importance**
The viral transactivating protein Tat has been shown to stimulate several steps of HIV gene expression. It was indeed found to facilitate reverse transcription. Moreover, Tat is strictly required for the transcription of viral genes. Although the presence of Tat within HIV virions would undoubtedly favour these steps and therefore enable the incoming virus to boost initial viral production, whether and how Tat is present within virions has been a matter a debate. We here described and characterized a tripartite complex between Tat, HIV capsid protein and the cellular chaperone cyclophilin A that enables efficient and specific Tat encapsidation within HIV virions. We further showed that Tat encapsidation is required for the virus to efficiently initiate infection and viral production. This effect is mainly due to the transcriptional activity of Tat.

**Keywords** HIV / Tat / Capsid / virions / Cyclophilin A

## Introduction

HIV virions contain key viral proteins needed to initiate infection. Indeed, HIV-enzymes such as reverse transcriptase that enables the production of viral cDNA and integrase that will insure insertion of this cDNA into cellular DNA are known to be encapsidated. After viral DNA integration, the next step of the infection cycle is transcription and, surprisingly, HIV transactivating protein Tat that is required for efficient transcription is not thought to be present into HIV virions (1). It is thus generally accepted that viral transcription becomes efficient, *i.e.* produces full length viral mRNAs, when neosynthesized Tat becomes available. Indeed, in the absence of Tat, viral transcription is poorly efficient (2) and it is not clear how Tat can be produced in the absence of Tat (3). In addition to transcription, Tat was also found to stimulate reverse transcription (4, 5). Biological relevance of this effect can only result from the presence of Tat within viral cores. A proteomic study identified Tat associated with purified HIV virions (6), but the specificity and mechanistic of Tat association to the viral particle remains to be established.

Cyclophilin A (CypA) is a chaperone of the prolylisomerase-immunophilin family. CypA is known to be encapsidated into HIV-1 virions (7) due to its affinity (Kd~16 µM) for the G89-P90 motif located within an exposed loop of the capsid protein (CA). The CA protein (24 kDa, p24) is produced during maturation of the Gag precursor polyprotein (55 kDa) by the viral protease. CypA binding to CA results in the incorporation of 200-250 molecules of CypA/virion, *i.e.* ~1 CypA/ 10 CA. The CA-G89V mutation in CA prevents CypA binding to CA and thus CypA encapsidation (8). In target cells, CypA binding to CA was found to protect the capsid from restriction by TRIM5α (9, 10). Interestingly, viruses deficient in CypA binding were found to be affected in reverse transcription efficiency, but the underlying mechanism remained to be uncovered (11).

Here we show that a tripartite complex Tat-CypA-CA forms in infected cells, that this complex can be purified, involves nanomolar affinities and enables efficient Tat encapsidation into HIV virions at the same level as CypA, *i.e.* 200-250 Tat molecules/virion. Encapsidated Tat strongly boosts transcription and also increases the efficiency of reverse transcription. Accordingly, encapsidated Tat stimulates by 5-10 folds HIV-1 infectivity and viral production in single round infection assays.

## Results

### Tat-CypA interaction does not require CypA active site

We previously observed using immunoprecipitation that HIV-1 Tat could interact with CypA (12). Here, we first examined whether Tat interaction with CypA relies on CypA catalytic site. To this end, we transfected HEK 293T cells with Tat or HIV-1 Gag as a control, and tested if they could be pulled-down form cell lysates by GST-CypA. We used as a control GST-CypA-H126Q. This point mutation within CypA active site was found to inhibit its enzymatic activity by > 99% (13) and to prevent its interaction with the NS5 protein of hepatitis C virus (14). While Gag (hence CA) could be efficiently pulled down from cell lysates by GST-CypA, it did not interact with GST-CypA-H126Q (Fig.1A, left panel). Surprisingly, the efficiency of Tat interaction with CypA-H126Q was ~42 % of the efficiency of Tat binding to WT CypA, while Tat only weakly interacted with GST (Fig.1A, right

panels). These data indicated that Tat can bind CypA independently of CypA active site, and suggest that a Tat-CypA-CA complex could exist within infected cells.

**A tripartite Tat-CypA-CA complex exists within cells**

We then examined whether a tripartite Tat-CypA-CA could be observed within transfected cells. We first used Tat-FLAG and anti-FLAG immunoprecipitation to isolate this complex from Tat-FLAG and Gag transfected cells. As shown earlier, CypA is co-immunoprecipitated with Tat (12), and this is observed whether Gag is present or not (Fig.1B). When Tat-FLAG and Gag were cotransfected, WT Gag but not Gag-CA-G89V was immunoprecipitated with Tat. These results suggested that a Tat-CypA-CA complex exists within cells and that, in this complex, CA and CypA interact *via* the well characterized binding interface, namely CypA active site and CA-Pro90 loop (8).

To confirm these data, we tried to pull-down the complex using GST-Tat and extracts from Gag transfected cells. GST-Tat, but not GST alone enabled to pull-down CypA and WT Gag (Fig.1C). Gag-CA-G89V could not be pulled-down by GST-Tat. CypA was pulled-down by GST-Tat in the presence of WT Gag only.

Altogether, these pull-down experiments showed that a Tat-CypA-CA complex can be detected in cell lysates. They thus suggest that this complex was formed in HEK 293T cells.

**Tat-CypA-CA complex can be purified by gel filtration**

We then assessed whether this complex could form using purified, untagged recombinant proteins (prepared as detailed in the Methods section). The three highly purified proteins could be separated by size exclusion chromatography (SEC). While CA and CypA eluted from the SEC column as sharp peaks at ~14 ml and ~17 ml (Fig.2A), Tat eluted as a very shallow peak at 19-20 ml (arrow in Fig.2A, top panel). When CA and CypA were mixed, the CA elution peak shifted to earlier retention times, indicating that a CA-CypA complex slightly but significantly bigger than CA alone was formed (Fig.2A middle panels; Fig.2B). This shift was not observed when CypA-H126Q was used (Fig.2A last panel; Fig.2B) indicating that this complex is a *bona fide* CA-CypA complex in which CypA is bound to CA via its catalytic site. This result is consistent with the inability of GST-CypA-H126Q to pull CA from cell extracts (Fig.1A). When Tat, CA and CypA were mixed then injected on the SEC column, the CA peak did not appear earlier compared to when CA+CypA were analyzed (compare the two middle panels in Fig.2A; Fig.2B), but when this fraction was analyzed by western blots we found that Tat was recruited at the level of the CA peak (Fig.2C). CypA-H126Q did not allow the recruitment of Tat to the CA peak. The CypA and Tat peaks only contain the cognate proteins. Hence, upon Tat + CypA injection, CypA did not recruit Tat to the CypA peak. Altogether these SEC results indicate that the ternary complex Tat-CypA-CA withstands gel filtration, while this is not the case for the Tat-CypA complex that seems more labile. This is consistent with binding affinity studies (see below). This SEC analysis thus confirmed the existence of the Tat-CypA-CA tripartite complex and indicated that it is stable, can be purified and amenable to biochemical characterization.

**Analysis of the Tat-CypA-CA complex by microscale thermophoresis**

To further characterize the complex and determine its interaction strengths we determined the dissociation constant at the equilibrium ($K_d$) of the three partners involved in the Tat-CypA-CA complex by microscale thermophoresis (MST). CypA, the central protein of the complex was fluorescently labeled. Labeled CypA interacted with CA with a $K_d$ of 8.3 ± 1.7 µM (Fig.3A) similar to the one reported before for the CypA-CA interaction (8), therefore indicating the functionality of fluorescent CypA. A preincubation of CypA with 1 µM Tat did not significantly affect CA-CypA interaction ($K_d$ of 5.5 ±0.25 µM). Tat affinity for CypA was higher ($K_d$ of 243 ± 23 nM) than that of CA for CypA. This is consistent with the observation that Tat-CypA interaction involves CypA regions that are apparently outside the active site (Fig.1A). Indeed, as a generalist chaperone, CypA exhibits a poor substrate specificity. The best substrates are those such as HIV-1 CA that contains the Gly-Pro motif (15) and their $K_d$ is > 5 µM (16). Tat submicromolar affinity for CypA thus indicates that Tat is not only interacting with CypA active site but makes more interfacial contacts (17). Interestingly, Tat affinity for CypA was enhanced 5- fold ($K_d$ of 55 ± 14 nM) when CypA was preincubated with 20 µM CA. This is consistent with SEC results (Fig.2).

**Analysis of the Tat-CypA-CA complex using surface plasmon resonance**

To confirm MST data we studied assembly of the Tat-CypA-CA complex using surface plasmon resonance (SPR). When Tat was immobilized on the chip before applying increasing doses of CypA, a strong interaction in the nM order was observed ($K_d$ of 255 ± 10 nM; Fig.3B, top left panel), in very good agreement with MST data. We did not observe any binding of CA to Tat (Fig. S1) while when a CypA+CA complex was applied to a Tat chip a $K_d$ of 95 nM was observed (Fig.3B, top right panel) indicating, as observed using MST, that Tat binds with more affinity to the CypA-CA complex than to CypA alone. The CA-CypA interaction has been studied extensively and, in agreement with previous measurements using SPR (8), we observed a $K_d$ of ~3.6 µM for CypA binding to CA (Fig.3B, bottom right panel). Nevertheless, when we followed CA binding to the Tat-CypA complex assembled on the chip, a $K_d$ of 110 ± 20 nM was obtained (Fig.3B, bottom left panel). Hence, SPR data indicated that the presence of Tat on CypA facilitates the CA-CypA interaction, while this was not observed using MST. Both techniques otherwise provided very consistent affinity constants (Fig.3C). They both indicated that Tat is preferentially recruited by CypA when CypA is already bound to CA. This suggests that Tat is preferentially recruited where CypA is bound to CA, and that the Tat-CypA-CA complex can thus drive Tat encapsidation.

**Tat is encapsidated in a CypA-dependent manner**

To examine whether the Tat-CypA-CA complex enables Tat encapsidation, we first purified HIV virions from transfected HEK 293T cells. Tat WT was observed in the purified WT virus preparation using two different monoclonal antibodies, a first one that recognize the N-ter (res 1-9) of the protein and a second that binds to a conformational epitope (18). A Tat mutant (Tat-W11Y) that poorly binds $PI(4,5)P_2$ (19) was also associated with the cognate virions; it was just not detected by the anti-Tat that recognizes the N-ter of the protein probably because the W11Y mutation severely inhibits the binding of this antibody (Fig.4A).

Hence, although HIV-1 budding takes place from PI(4,5)$P_2$ enriched area of the plasma membrane and virions are accordingly enriched in this phosphoinositide (20), these results indicate that Tat binding to PI(4,5)$P_2$ is not required for Tat association with purified virions. Non palmitoylable Tat (Tat-C31S (Chopard *et al*, 2018)) was also encapsidated, although this mutant was also less efficiently recognized by the N-ter anti-Tat. This result indicated that Tat palmitoylation is not required for Tat encapsidation. Very low amounts of Tat could be detected in CA-G89V virions even upon overexposure and the amount of Tat associated with these virions usually represented less than 5% of that present in WT virions. In agreement with previous studies (21, 22), viruses with CA-G89V did not incorporate CypA. The immunophilin FKBP12 that is weakly encapsidated (~25 copies/virions (23)) and that can interact with Tat (12) was also present in CA-G89V virions. Altogether these results indicated that, in agreement with biochemical data, Tat encapsidation relies on the presence of encapsidated CypA, while Tat interaction with PI(4,5)P2 or FKBP12 does not seem to allow significant Tat encapsidation. This CypA-dependent Tat encapsidation also indicates that the presence of Tat in purified virus preparations is not the result of contamination by exosomes or other cell-derived vesicles. Encapsidated Tat was quantified using semiquantitative blots (Fig. S2). A calculation based on p24 quantification by ELISA of purified virions and the number of 2000-2500 CA per virion (24) showed that 200-250 Tat molecules were present by virion, just as it is the case for CypA (8). This result is consistent with the high affinity of Tat for CypA-CA ($K_d$ 55-95 nM; Fig.3C) compared to the 38-150 lower affinity of CypA for CA (3.6-8.3 µM; Fig.3A-B). Hence, the limiting factor for Tat encapsidation is CypA binding to CA, and not Tat binding to CypA.

It was important to validate this CypA-dependent Tat encapsidation using viruses obtained following infection. We thus analyzed HIV-1 virions purified from infected Jurkat T-cells (Fig.4B). For these viruses produced by infected T-cells, Tat was present in WT viruses as a doublet. While the major band represents full-length Tat (two-exon) of 101 residues, the minor band probably corresponds to the single-exon form of Tat (72 residues (25)) that is also produced during infection (26). Tat incorporation was strongly decreased when CypA encapsidation was inhibited by the CA-G89V mutation or when infected cells were treated with cyclosporin-A (CSA) a CypA inhibitor that prevents its interaction with CA (27) and CypA encapsidation (7, 28). The result that both two- and single-exon Tat can be encapsidated suggests that Tat encapsidation motif, *i.e.* Tat CypA-binding site, resides within the first 72 residues of the protein.

To further check whether Tat was associated with HIV capsid cores we isolated cores from purified HIV-1 virions treated with Triton X-100 to dissolve the viral envelope (29). The absence of HIV matrix protein (MA, p17) and gp120 from purified capsid cores (Fig.4C) indicated that the viral envelope was efficiently removed by the treatment with a non-ionic detergent, as reported earlier (30). Tat and CypA association with purified cores was observed for WT viruses but not for CA-G89V or viruses from CSA-treated cells (Fig.4C), indicating that the association of Tat with viral cores requires CypA. This experiment confirms that Tat is not encapsidated by binding to PI(4,5)$P_2$ since, if this was the case, it would have been removed from the cores by the detergent as it is the case for MA that is bound to PI(4,5)$P_2$ (31).

Altogether, these biochemical data indicated that Tat is encapsidated by HIV-1 in a CypA-dependent manner.
To confirm these biochemical observations, we used a morphological approach. We examined virions using a correlative atomic force / total internal reflection fluorescence microscopy (AFM/TIRF) setup (32). This approach enables to identify viruses stringently using both TIRF to visualize the presence of Gag, and AFM to monitor the size of HIV-1 virions, *i.e.* 100-120 nm (24). Freshly purified virions plated on coverslips were permeabilized for immunofluorescence labeling of Tat and CA. Virions were identified as round-shaped particles with height > 100 nm by AFM, and fluorescent CA labeling by TIRF. Tat was observed in >90% of WT virions but only of 18% of CA-G89V viruses (Fig.4D).

Altogether, biochemical and morphological data showed that Tat is encapsidated in a CypA-CA dependent manner.

**Encapsidated HIV-1 Tat is delivered to the cytosol**

We then assessed whether encapsidated Tat is delivered to the cytosol upon infection. To examine this point, we transfected human primary CD4 T-cells with an LTR-firefly luciferase vector whose transcription is activated by Tat and a renilla control vector, before adding VSV-G pseudotyped ΔEnv viruses. To specifically follow the cytosolic delivery of encapsidated Tat and prevent Tat synthesis by infected cells, azidothymidine (AZT) was used to inhibit reverse transcription. Transactivation by Tat was followed using the firefly/renilla activity ratio (Fig.5A). The absence of encapsidated Tat induced a ~60% or ~80 % decrease in firefly production for CA-G89V viruses or viruses from CSA treated cells, respectively. This result indicated that Tat encapsidated by WT viruses is delivered to the cytosol upon infection and is transcriptionally active.

**Encapsidated Tat seems to be required for HIV-1 infectivity**

Since encapsidated Tat is delivered to the cytosol and transcriptionally active, it should enable the virus to establish infection more quickly and efficiently. We examined the effect of encapsidated Tat on infection by HIV-1 using single-round infectivity assays (33). To this end, Jurkat T-cells were infected using VSV-G pseudotyped ΔEnv viruses, either WT, CA-G89V or from CSA-treated cells. Results from p24 intracellular staining (FACS analysis) showed that for the highest MOI, cell infection monitored using p24 was reduced by 60% or 40% when Tat was removed from virions using CSA or CA-G89V, respectively (Fig.5B). When viral production was monitored using p24 ELISA, a reduction of 95% and 80% for CSA or CA-G89V viruses was observed (Fig.5C). When human primary CD4 T-cells were used as targets, whatever the MOI, viruses without encapsidated Tat were ~five-fold (CSA) or more than 10-fold (CA-G89V) less infectious than WT HIV-1 (Fig.5D). Similar data were obtained when viral production was monitored (Fig.5E). The reduced toxicity of viruses with the CA-G89V or prepared from CSA-treated cells was reported earlier by different groups (21, 34).
Altogether single-round infection assays using CA-G89V and especially CSA-viruses suggested that encapsidated Tat is important to establish both efficient infection and sustained viral production.

**Encapsidated Tat seems to facilitate viral reverse transcription and integration**

We then examined using CA-G89V and CSA-viruses at which stage encapsidated Tat could act to favor infection. Regarding early steps of the infection cycle, Tat was found to facilitate reverse transcription (4, 5, 35) and CypA was found to be required for the initiation of reverse transcription (36). We therefore examined whether encapsidated Tat affected the production of early and late reverse-transcription products. We quantified these products by qPCR 6 h following infection, when their production is high (37). The reverse transcription activity of both CSA-viruses and CA-G89V virions was only ~50% compared to control viruses (Fig.6A). In agreement with RT data, the integration of viral DNA was similarly affected by 30-70% when encapsidated Tat was absent (Fig.6B).

**Encapsidated Tat strongly stimulates transcription**

Tat is required for the efficient transcription of viral genes (3). We examined by qRT-PCR of intracellular viral RNA to what extend encapsidated Tat could affect viral transcription at 24 h and 34 h post-infection, *i.e.* following the integration of viral DNA (37). We used a set of primers that enables to quantify long transcripts (~5.3 kb from the transcription start site) whose production is strongly Tat-dependent (38). Transcription efficiencies were corrected for the integration efficacy of each virus (Fig.6B). Viruses without encapsidated Tat (CSA or CA-G89V) were strongly affected in viral transcription whose efficiency was only 0.3-3 % of that of WT viruses for both time points (Fig.6C). Hence the presence of encapsidated Tat strongly boosts transcription at the beginning of infection.

**Complementation of Tat-deficient viruses confirms the role of encapsidated Tat in infection**

As indicated above, the CSA and CA-G89V viruses are devoid of encapsidated Tat but also of CypA and, furthermore, the CA-G89V mutant is unable to bind CypA. To specifically examine the role of encapsidated Tat in infection, we prepared viruses with CypA and different versions of Tat either WT, or with a point mutation reported to selectively inactivate transcription (Tat-C22S (39)) or reverse transcription (Tat-Y47H (40)). According to an RMN-based structure (41) the mutated residues are, except for the hydroxyl group of Y47, located inside the protein. Their mutation was thus unlikely to affect CypA binding and Tat encapsidation. Viruses were produced using a ΔEnv ΔTat viral clone that was cotransfected in HEK 293T cells with Tat and VSV-G vectors. An issue with this approach is that transcriptionally-active Tat is needed to produce HIV virions. WT Tat was thus co-transfected 1/2 with Tat-C22S (and Tat-Y47H) mutants to insure significant viral production by Tat-C22S virions. Biochemical analyses of the virions showed that they contained equivalent amounts of CA and CypA. Tat-Y47H was encapsidated as efficiently as WT Tat, while Tat-C22S, that exhibits a change in electrophoretic mobility, was more efficiently encapsidated (Fig.7A). We first examined whether these mutations were specific by infecting Jurkat cells with these complemented ΔTat viruses in single-round assays and monitoring the production of RT products and long HIV-RNAs. We found that viruses with encapsidated Tat-Y47H were affected in reverse transcription (-60 %; Fig.7B), and integration (-40 %; Fig.7C). They

were less affected in their transcriptional activity (-30%; Fig.7D). Conversely, viruses with encapsidated Tat-C22S were essentially and strongly affected in transcription (-90%; Fig.7D). In agreement with data from single mutants, viruses with the double mutant Tat-C22S-Y47H were strongly affected in reverse transcription, integration and transcription (decreased by 60-90%).

We then monitored infection and viral production by these viruses that have a mutated-encapsidated Tat. Although the Tat-C22S mutation decreased the efficiency of infection (Fig.7E) and viral production (Fig.7F) by ~90 %, the Tat-Y47H mutation inhibited infection and viral production by 65-70%. Virions with the double mutant Tat-22S-47H behave as those with Tat-C22S. Altogether, these studies of complemented ΔTat viruses (Fig.7) provide compelling evidence that the ability of encapsidated Tat to stimulate reverse transcription, and especially transcription are involved in HIV infectivity.

To confirm these data based on the complementation of ΔTat viruses, we prepared viruses in which we encapsidated Tat using Vpr fusions. Fusion with the viral protein Vpr that is efficiently encapsidated is an efficient method to encapsidate proteins into HIV virions (42). To prepare viruses that only contains Tat as a Vpr fusion protein we had to use as template a virus without encapsidated Tat, and to this end we used HIV-CA-G89V (Fig.4). We made Tat-Vpr fusions using WT, C22S, Y47H or 22S-47H versions of Tat, and CypA-Vpr was used as a negative control. The corresponding plasmids were cotransfected with ΔEnv pNL4.3-CA-G89V and pVSV-G to obtain pseudotyped viruses. Biochemical analysis of the virions showed that Vpr chimera were encapsidated to similar levels (Fig.8A). In single-round infection assays, the most efficient infection and viral production were observed for the virions with Tat-Vpr (Figs.8B-C). The negative control CypA-Vpr level represents the participation of neosynthesized Tat in p24 intracellular staining (% infection) and viral production. The Tat-C22S mutation essentially ablated viral production due to Vpr-Tat (-85 %, Fig.8C), while the Tat-Y47H mutation had a milder effect on viral production (-45%; Fig.7F). The double mutant Tat-22S-47H behaved essentially as the Tat-C22S transcription-inactive mutant.

Altogether, single-round infection data of ΔTat complemented viruses and VPR-chimeras confirmed that encapsidated Tat is required for viral production, especially to boost transcriptional activity.

**Discussion**

The CypA-binding loop within HIV capsid protein has several key roles within the infected cell. First, CypA binding protects HIV-1 core from the TRIM5α restriction factor (9, 10). The absence of CypA on CA-G89V capsids thus triggers restriction by TRIM5α, but this effect is only observed in primary T-cells (9) and not in transformed cells (43) such as Jurkat cells (10). Hence, it is likely that the CA-G89V mutant infects less efficiently primary CD4 T-cells (Fig.5D-E) than the Jurkat cell line (Fig.5B-C) due to restriction by TRIM5α. The presence of CypA on the incoming capsid is also essential for the action of the nuclear envelope protein SUN2 that is needed for HIV infection (44). Moreover, the CypA binding loop from CA is involved in capsid nuclear import by binding to the cytoplasmic nuclear pore complex protein Nup358/RanBP2 (22) and transportin-1 (45).

Here we document another role of this CypA-binding loop, that acts at the level of nascent virions by enabling Tat encapsidation *via* the formation of a CA-CypA-Tat tripartite complex. Some reports indicated that Tat could be associated with HIV virions. Tat was detected in a proteomic study of purified HIV viruses, but no quantification was made (6). A potential caveat with Tat is that it is actively secreted by infected cells (19, 46) and that Tat association with viral particles could therefore take place after viral budding and be potentially non-specific. Nevertheless, a gp120-Tat high affinity interaction was observed (47). The presence of Tat specifically or unspecifically bound to virion surface might be responsible for the presence of Tat at low levels in viruses from CA-G89V mutants or CSA-treated cells, but this is a very minor fraction of virion-associated Tat that is encapsidated in a CypA-dependent manner (Fig.4).

Throughout this study we monitored HIV infectivity using single-round assays to specifically examine the role of encapsidated Tat in the initial steps of infection. We used different complementary approaches and viruses, such as viruses from CSA-treated cells, ΔTat complemented viruses and viruses containing Vpr-Tat fusions. All approaches provided essentially the same results. They confirmed the role of Tat (4, 5, 35) on reverse transcription, but the effect of encapsidated Tat on the RT step was less pronounced than that on the transcription of viral genes that enables to efficiently initiate viral production before neosynthesized Tat becomes available.

Indeed, viruses devoid of transcriptionally-active encapsidated Tat showed very weak transcriptional activity after 24h of infection. It ranged from 3% for CSA-viruses (Fig.6C) to <10% for ΔTat viruses complemented with Tat-C22S (Fig.7D).

Viruses prepared from CSA-treated cells have native CA that can bind cytosolic CypA upon cytosolic delivery, likely preventing recognition by restriction factors such as TRIM5α that binds to CypA loop on capsid cores with very low affinity compared to CypA (48). Hence, the defect in transcription of CSA-viruses is likely due to the lack of encapsidated Tat and not CypA, especially since viral transcription is a post-integration event that takes place in a CypA-containing cell. This interpretation was confirmed by the use of complemented ΔTat viruses (Fig.7). Hence, the difference of infectivity between CSA and WT viruses probably relies on the presence of Tat in WT virions. The lack of transcriptionally-active encapsidated Tat induces a loss of infectivity and viral production of 70-95 % whatever the viruses and the target cells (Fig.5,7 and 8).

We observed that 200-250 copies of Tat are associated with virions. This number of molecules in the human T-cell volume of 176 $\mu m^3$ (49) generates a Tat concentration of ~2 nM, above the Kd (0.4-0.8 nM) involved in the assembly on HIV transcription complex Tat-pTEFb-TAR (50). Each HIV virus therefore encapsidates enough Tat to efficiently stimulate transcription. While recent data showed that HIV-1 capsid remains intact until it enters the nucleus (51), live-cell imaging indicated that CypA dissociates from the capsid upon nuclear entry (52). Hence, upon HIV entry, Tat should be delivered within or at the nuclear doorstep so that Tat is present close to its action site.

Here we show that, by encapsidating Tat, HIV can take control of transcription from the beginning, so that this key step of viral gene expression is efficient as early as possible. The

virus thus encapsidates the three viral proteins, reverse transcriptase, integrase and Tat that are needed to initiate the production of viral RNA and proteins.

## Materials and methods

### Materials

Opti-MEM, Lipofectamine 2000, media and sera for cells were from Life technologies. Oligonucleotides and most usual chemicals were from Merck-Millipore. CSA was from Clinisciences (CB0352) and AZT from the HIV reagent program (#3485). The antibodies used in this study are listed in Table S1.

### Recombinant proteins

Recombinant Tat (86 residues, BH10 isolate) was produced and purified from transformed *E.coli* as described (53). Tat of 101 residues was also produced but the yield was much lower and it was only used as a standard for SDS/PAGE.

Recombinant human CypA was produced using a pET vector encoding a N-terminal $His_6$ tag before a TEV protease site (ENLYFQG) and CypA coding sequence (54). After growing transformed BL21 λDE3 *E. coli* cells at 37°C for 4 h, bacteria were lysed by sonication in 150 mM NaCl 150 mM, 10 mM imidazole, 1 mM DTT, 50 mM Tris, pH 8.0 supplemented with antiproteases (Complete$^c$, Roche) and 1 mg lysozyme / ml. The lysate was clarified by centrifugation before adding Ni-NTA-agarose (Qiagen) and incubation for 2 h at 4°C on a rotating wheel. The resin was then transferred to a column and washed with lysis buffer supplemented with 10 mM imidazole. His6-CypA was eluted with 500 mM imidazole in lysis buffer, then dialyzed overnight at 4°C against 150 mM NaCl, 50 mM Tris, pH 8.0, containing 1mM beta mercaptoethanol together with $His_6$-TEV protease (1 mg / 50 mg of His6-CypA). Ni-NTA-agarose was then added to the dialysate to remove $His_6$-TEV protease and any unprocessed $His_6$-CypA. After 2 h at 4°C on a wheel and centrifugation, the supernatant containing purified CypA was collected. It contains processed CypA that only has an extra N-terminal gly residue, and that was aliquoted and stored at -80°C.
Purification of the CA protein from transformed *E.coli* was performed as described (55). CypA-H126Q and CA-G89V pET vectors were generated using a quickchange lightning kit (Agilent); coding sequences were entirely sequenced and proteins were purified as described above for the WT proteins.
GST-tagged proteins were purified essentially as described (56). Briefly, E coli BL21 cells transformed with pGEX vectors containing Tat101 (57), CypA or CypA-H126Q (58) were grown at 37°C until OD=0.6. Production of GST-tagged protein was induced by adding 1 mM isopropylthiogalactoside for 4.5 h at 30°C. Bacteria were then lysed in 150 mM NaCl, 50 mM Tris pH 7.5 supplemented with antiproteases, 0.5% TX-100 and 2 mM DTT. After sonication for 1 min, bacterial extracts were centrifugated for 20 min at 18,000 x g at 4°C and the supernatant was incubated with 1.5 ml of a GSH-sepharose 4B resin (GE Healthcare 17-0756-01) for 1.5 h at 4°C on a rotating wheel. After washing with lysis buffer, beads were frozen in lysis buffer supplemented with 10% glycerol and stored as aliquots at -80°C.

**SEC experiments**

CypA and CA were dialysed against gel filtration buffer (150 mM NaCl, 5 mM DTT, 50 mM citrate, pH 7.3), while lyophilized Tat was resuspended in this buffer. Proteins (18 nmoles each in 250 µl buffer) were incubated for 30 min at RT then loaded on a Superdex 200 Increase 10/300 GL column connected to an AKTA purification system (GE Healthcare). The column (bed volume 24 ml; void volume 8.8 ml) was equilibrated and eluted at 0.4 ml/min in gel filtration buffer. Fractions (0.5 ml) corresponding to chromatographic peaks (identified using $ABS_{280}$) were pooled before precipitation with 33% trichloroacetic acid for 30 min on ice. Pellets were washed with ice-cold acetone, then resuspended in reducing sample buffer before SDS/PAGE and western blots against Tat, CypA and CA.

**Microscale thermophoresis (MST)**

Proteins were dialyzed overnight against 150 mM NaCl, 50 mM citrate, pH 7.3 the day before the experiment. CypA (WT or H126Q) were labeled with the Monolith Protein Labeling Kit RED-NHS $2^{nd}$ generation according to the recommendations of the manufacturer (NanoTemper Technologies). Briefly, CypA (200 µl at 10 µM) was labeled with 5 µl of labeling reagent. After 30 min the mixture was loaded on a minitrap-G25 column (GE Healthcare) and the labeled protein was eluted with 300 µl of dialysis buffer. Labeled CypA was used at 50 nM and dilutions were made in dialysis buffer containing 0.05% Tween. Protein-protein interactions were analyzed at 20°C by MST on a Monolith NT.115 (NanoTemper technologies) using standard capillaries. We made controls recommended by the manufacturer. Absence of aggregation or interaction with the capillary glass was checked by assessing the MST signal traces and the homogeneity of the fluorescence curve from the capillary scan. We also monitored that the fluorescence signal was homogeneous along all capillaries. Measurements were repeated at least two times. $K_d$ values were calculated using the NTAnalysis software (NanoTemper technologies) or GraphPad Prism.

**Surface Plasmon Resonance**

The Surface Plasmon Resonance experiments were performed at 25 °C on a T200 apparatus (Cytiva) using a buffer containing 150 mM NaCl ,20 mM phosphate and 30 mM citrate, pH 7.0 and supplemented with 0.05% P20 surfactant (Cytiva). CA and Tat Proteins at 50 µg/ml in 150 mM NaCl, 50 mM acetate pH 5.0 and 150 mM NaCl, 50 mM citrate pH 6.2, respectively, were immobilized on aCM5S sensor chip by amine coupling according to the manufacturer's instructions. Around 11000 RU of Tat and 1000 RU of CA were thereby immobilized. Affinities were estimated by one cycle kinetic titration at five increasing concentrations (370-6000 nM, two fold dilution series) of CypA, equimolecular CypA /CA mixing, or CA injected on 50-70 RU of CypA previously bound on immobilized Tat. A two-state fitting model (BIAevaluation software 4.1; Cytiva) was used for calculations. No binding of CypA was observed on CA-G89V (Fig. S1).

**Cells and transfections**

Cell lines were obtained from the ATCC and cultivated following their recommendations. They were checked monthly for mycoplasma contamination. Jurkat cells (ATCC clone E6-1, TIB-152) were transfected by electroporation using Amaxa kit V (program X-005), and HEK

293 T (ATCC CRL-11268) were transfected using PEImax as described (59). The pCI vector (Promega) was used as control vector except otherwise indicated.
For the preparation of human T-cells, human blood from healthy donors was obtained from the local blood bank (Etablissement Français du Sang, Montpellier; agreement 21PLER2019-0106). Peripheral blood mononuclear cells were isolated by separation on Ficoll-Hypaque (Eurobio). CD4+ T-cells were then purified using a CD4 Easysep negative selection kit (Stemcell). They were activated using phytohemagglutinin (1 µg/ml) for 24 h then interleukin-2 (50U/ml) for 4-6 days before nucleofection (as recommended by the manufacturer, Lonza) or infection by HIV-1.

**GST-pull downs**

Transfected HEK 293T cells (~7.5 x $10^6$ cells) were scraped, washed with PBS, then lysed on ice in 0.5 ml of 150 mM NaCl, 20 mM $NaH_2PO_4$, 30 mM citrate, pH 7.4 supplemented with antiprotease (Complete, Roche) and 1% Triton X-100. The lysate was sonicated (~10 Watts) on ice for 30 sec using 5 sec pulses, then cleared by centrifugation (3 min at 20.000 x g, 4°C). GST beads (~15 µl) were washed twice in lysis buffer and added to the cleared cell lysates. After 2 h at 4°C on a rotating wheel, the resin was washed 4-fold in lysis buffer, then resuspended in reducing sample buffer for SDS/PAGE (tricine gels with 10% acrylamide) and blotting on a nitrocellulose membrane.

**Immunoprecipitations**

HEK 293T cells were transfected with a Tat-FLAG expression vector with or without a Gag vector. Cells (~7.5 x $10^6$ cells) were lysed in 0.5 ml of lysis buffer as described for GST-pull downs. Anti-FLAG magnetic beads (Sigma M8823; ~10 µl) were washed twice in lysis buffer and added to the cell lysates. After 90 min at 4°C on a rotating wheel, the resin was washed 4-fold in lysis buffer, then resuspended in reducing sample buffer for SDS/PAGE and western blotting.

**Viruses and infections**

To produce HIV-1 virions, HEK 293 T cells were transfected with pNL4.3 using PEI max (12). To prepare pseudotyped viruses, cells were cotransfected (ratio 1:5) with a pCMV-VSV-G vector and a ΔEnv pNL4.3. The latter was obtained by deletion between the NdeI (6399) and ApaLI (6610) restriction sites of pNL4.3. This deletion introduced a stop codon so that a truncated protein of 63 residues only was produced instead of the 854 residues Env protein. Vpu sequence was not altered. The ΔTat pNL4.3 clone has been described (12) and ΔTat ΔEnv pNL4.3 was produced as described above.
Vpr chimera were constructed by PCR amplification of Vpr (60), CypA or Tat in pCi vector (Promega) and mutations were introduced using QuickChange lightning. Coding sequences were entirely sequenced.
For the complementation of the ΔTat virus, ΔTat ΔEnv pNL4.3 was cotransfected with pCMV-VSV-G (6/1 ratio) and 1/1000 of the indicated pBi-Tat vector. To prepare ΔTat viruses complemented with Tat mutants a cotransfection WT Tat / mutant Tat (1/2) was used.

This procedure allowed viral production when using the Tat-C22S mutant that is transcriptionally inactive (39).
For the production of viruses with Vpr chimera, HEK293T cells were cotransfected with CA-G89V ΔEnv pNL4.3, Tat-Vpr or CypA-Vpr (3/1 ratio) and pCMV-VSV-G vector (5/1 ratio). When indicated transfected cells were treated with 2 µM CSA to prevent CypA encapsidation (7, 28). These viruses were termed CSA-viruses throughout this paper. The cell supernatant was harvested 48h after transfection, filtered onto 0.4 µm filters and ultracentrifugated on 20% sucrose at 125 000 x g for 2 h at 4°C. Viruses were resuspended in PBS, allowed to stand for 1h on ice, then aliquoted and stored at -80°C. Virus titers were determined by ELISA p24 (Innotest) using appropriate standards. WT CA and CA-G89V were similarly detected using this ELISA kit (Fig. S4), and viral stocks were normalized using p24 ELISA. Single round infections were performed using 3-300 ng p24 of VSV-G pseudotyped viruses per million T-cell. 18h after infection, cells were washed three times in culture medium then resuspended in fresh medium that was harvested 18 h later for p24 ELISA. Negative controls included 20 µM AZT. For FACS analysis cells were stained for p24 using Kc57-RD1 or Kc57-FITC and analysed using an ACEA NovoCyte flow cytometer. This antibody similarly detected WT CA and CA-G89V (Fig. S5).

For Tat delivery experiments, human primary $CD4^+$ T-cells were transfected with a LTR-Firefly luciferase vector and a control TK-Renilla luciferase vector (53). Transfection was performed using Amaxa kit VPA-1002, as described by the manufacturer. After 18 h, cells were infected using 300 ng p24 of VSV-G pseudotyped viruses per million T-cell. AZT (20 µM) was used to block reverse transcription. Cells were harvested after 24h for luciferase assays (Dual-Glo luciferase assay, Promega). Results are expressed as Firefly/Renilla activity ratio.

**Capsid core purification**

Capsid cores were purified as described (29). Briefly, freshly-purified virions were resuspended in ice-cold 0.1 M MOPS (3-(N-morpholino) propane sulfonic acid), pH 7.0, and Triton X-100 was then added at 0.5% final concentration. After 2 min at 4°C, viral cores were centrifugated at 20,000 × g for 8 min at 4°C. Pellets were washed twice with 0.1M MOPS and cores were finally resuspended in SDS/PAGE sample buffer for western blots.

**TIRF and AFM microscopy**

Coverslips were first cleaned by bath sonication in 1M KOH, then rinsed, sonicated in ultrapure water, then treated with 10 mM $NiCl_2$ for 1 h at RT. Freshly isolated viruses (WT or CA-G89V) were diluted 10-fold in PBS then applied to coverslips that were then incubated for 15 min at 37°C before fixation with 3.7 % paraformaldehyde in PBS. Following fixative neutralization with 50 mM $NH_4Cl$, viruses were permeabilized with 0.05% saponin in PBS containing 1% bovine serum albumin, then labelled with rabbit anti-Tat and goat anti-p24 for 30 min, then with donkey anti-goat-alexaFluor647 and swine anti-rabbit-FITC for 30 min. Viruses were imaged within 24h with an MSNL Bruker microlever probe using an AFM microscope (Nanowizard 4, JPK Instrument) coupled with a fluorescence microscope (Axio observer, Carl Zeiss) equipped with a 63x NA1.4 objective and operated in the TIRF mode. Images were 50 µm x 50 µm (512 x 512 pixels). AFM and TIRF images were aligned using

the Ec-CLEM Icy plug-in (61) and colocalization was assessed using Imaris setting a threshold of 300 nm, which is about the diffraction limit of the fluorochromes. Viruses were identified as $CA^+$ TIRF spots with an AFM signal whose height >100 nm.

**qPCR and qRT-PCR**

Jurkat cells were infected with VSV-G pseudotyped viruses (WT, CSA or CA-G89V; 15.3 ng p24/ million cells). Cells were pelleted for DNA extraction using QIAamp- DNA-MiniKit (Qiagen) 6, 24 or 34 h after infection. For RNA extraction, cells were harvested 24 h or 34 h after infection, washed three times with PBS containing 1% FBS, before extracting RNA using Trizol (Thermofisher). Extractions were performed following the manufacturer instructions. Early and late RT products as well as integrated viral DNA were quantified exactly as described (62) using TaqMan Universal Master Mix II (Applied Biosystems). To generate a standard curve for Alu-PCR, Jurkat cells were infected using high-titer pseudotyped WT or CA-G89V virus and maintained for 1 month in culture so that extrachromosomal forms of viral DNA were lost (37). Standard qPCR curves for the quantification of RT products were obtained using linearized pNL4.3.

To monitor HIV transcription, RNA was reverse transcribed into first-strand cDNA using All-in-one RT MasterMix (Applied Biological Materials). qPCR of cDNA was then performed using P7/P8 primers (amplified fragment is nucleotides 5249-5358 of HIV NL4.3 genome), LightCycler 480 SYBR Green I Master mix (Roche) and normalization using GAPDH as described (38). Identical amounts of DNA (~20 ng) was used for each reaction.

**Statistics and data access**

Data were analyzed for statistical significance using Prism 8.4. All data related to this study are available upon request to the corresponding author.

**Acknowledgements**

This work was funded by Sidaction (2019-AEQ-12183) to BB, FRM (Equipe FRM 20161136701) to JMM, FranceBioImaging (FBI, ANR10INSB04) and the GIS IBISA (Infrastructures en Biologie Santé et Agronomie) to PEM. We are grateful to Husam Alsarraf and Aurélien Thureau for help during SEC experiments, Jean-Jacques Bono and Virginie Gasciolli for assistance during thermophoresis experiments, Christophe Chopard and Xavier Hanoulle for pioneer experiments, Juliette Cuminal, Chainez Benhacine and Melissa Ramos Mach for technical assistance, Laurent Chaloin and Jean-Marie Peloponese for expertise in structural biology and qRT-PCR, respectively.

**Author contributions**

MS, CO, LM and IC performed *in cellulo* protein interaction studies. MS and CO performed SEC analysis supervised by MB. MS, JFG and MB performed thermophoresis analysis. MP and CH analyzed interactions using Biacore. VT, CO and LM analyzed purified virions and capsids. MS, LC, CG and PEM performed TIRF/AFM experiments. CM prepared all HIV mutants. MS, CO, LM and BB performed infectivity studies. JMM provided funding and scientific input. BB supervised the study and wrote the manuscript with inputs from all the authors.

The authors declare that they have no conflict of interest.

## References


1. Swanson CM, Malim MH. 2008. SnapShot: HIV-1 proteins. Cell 133:742, 742.e1.
2. Feinberg MB, Baltimore D, Frankel AD. 1991. The role of Tat in the human immunodeficiency virus life cycle indicates a primary effect on transcriptional elongation. Proc Natl Acad Sci U S A 88:4045-9.
3. Ott M, Geyer M, Zhou Q. 2011. The control of HIV transcription: keeping RNA polymerase II on track. Cell Host Microbe 10:426-35.
4. Harrich D, Ulich C, Garcia-Martinez LF, Gaynor RB. 1997. Tat is required for efficient HIV-1 reverse transcription. Embo J 16:1224-35.
5. Boudier C, Humbert N, Chaminade F, Chen Y, de Rocquigny H, Godet J, Mauffret O, Fosse P, Mely Y. 2014. Dynamic interactions of the HIV-1 Tat with nucleic acids are critical for Tat activity in reverse transcription. Nucleic acids research 42:1065-78.
6. Chertova E, Chertov O, Coren LV, Roser JD, Trubey CM, Bess JW, Jr., Sowder RC, 2nd, Barsov E, Hood BL, Fisher RJ, Nagashima K, Conrads TP, Veenstra TD, Lifson JD, Ott DE. 2006. Proteomic and biochemical analysis of purified human immunodeficiency virus type 1 produced from infected monocyte-derived macrophages. J Virol 80:9039-52.
7. Franke EK, Yuan HE, Luban J. 1994. Specific incorporation of cyclophilin A into HIV-1 virions. Nature 372:359-62.
8. Yoo S, Myszka DG, Yeh C, McMurray M, Hill CP, Sundquist WI. 1997. Molecular recognition in the HIV-1 capsid/cyclophilin A complex. J Mol Biol 269:780-95.
9. Kim K, Dauphin A, Komurlu S, McCauley SM, Yurkovetskiy L, Carbone C, Diehl WE, Strambio-De-Castillia C, Campbell EM, Luban J. 2019. Cyclophilin A protects HIV-1 from restriction by human TRIM5alpha. Nat Microbiol 4:2044-2051.
10. Selyutina A, Persaud M, Simons LM, Bulnes-Ramos A, Buffone C, Martinez-Lopez A, Scoca V, Di Nunzio F, Hiatt J, Marson A, Krogan NJ, Hultquist JF, Diaz-Griffero F. 2020. Cyclophilin A Prevents HIV-1 Restriction in Lymphocytes by Blocking Human TRIM5alpha Binding to the Viral Core. Cell Rep 30:3766-3777 e6.
11. De Iaco A, Luban J. 2014. Cyclophilin A promotes HIV-1 reverse transcription but its effect on transduction correlates best with its effect on nuclear entry of viral cDNA. Retrovirology 11:11.
12. Chopard C, Tong PBV, Toth P, Schatz M, Yezid H, Debaisieux S, Mettling C, Gross A, Pugniere M, Tu A, Strub J-M, Mesnard J-M, Vitale N, Beaumelle B. 2018. Cyclophilin A enables specific HIV-1 Tat palmitoylation and accumulation in uninfected cells. Nature communications 9:2251.
13. Zydowsky LD, Etzkorn FA, Chang HY, Ferguson SB, Stolz LA, Ho SI, Walsh CT. 1992. Active site mutants of human cyclophilin A separate peptidyl-prolyl isomerase activity from cyclosporin A binding and calcineurin inhibition. Protein science 1:1092-9.
14. Foster TL, Gallay P, Stonehouse NJ, Harris M. 2011. Cyclophilin A interacts with domain II of hepatitis C virus NS5A and stimulates RNA binding in an isomerase-dependent manner. J Virol 85:7460-4.
15. Howard BR, Vajdos FF, Li S, Sundquist WI, Hill CP. 2003. Structural insights into the catalytic mechanism of cyclophilin A. Nature structural biology 10:475-81.
16. Piotukh K, Gu W, Kofler M, Labudde D, Helms V, Freund C. 2005. Cyclophilin A binds to linear peptide motifs containing a consensus that is present in many human proteins. The Journal of biological chemistry 280:23668-74.

17. Vangone A, Bonvin AM. 2015. Contacts-based prediction of binding affinity in protein-protein complexes. Elife 4:e07454.
18. Mediouni S, Watkins JD, Pierres M, Bole A, Loret EP, Baillat G. 2012. A monoclonal antibody directed against a conformational epitope of the HIV-1 trans-activator (Tat) protein neutralizes cross-clade. The Journal of biological chemistry 287:11942-50.
19. Rayne F, Debaisieux S, Yezid H, Lin YL, Mettling C, Konate K, Chazal N, Arold ST, Pugniere M, Sanchez F, Bonhoure A, Briant L, Loret E, Roy C, Beaumelle B. 2010. Phosphatidylinositol-(4,5)-bisphosphate enables efficient secretion of HIV-1 Tat by infected T-cells. EMBO J 29:1348-62.
20. Sundquist WI, Krausslich H-G. 2012. HIV-1 assembly, budding, and maturation. Cold Spring Harbor perspectives in medicine 2:a006924.
21. Sokolskaja E, Sayah DM, Luban J. 2004. Target cell cyclophilin A modulates human immunodeficiency virus type 1 infectivity. Journal of virology 78:12800-8.
22. Schaller T, Ocwieja KE, Rasaiyaah J, Price AJ, Brady TL, Roth SL, Hue S, Fletcher AJ, Lee K, KewalRamani VN, Noursadeghi M, Jenner RG, James LC, Bushman FD, Towers GJ. 2011. HIV-1 capsid-cyclophilin interactions determine nuclear import pathway, integration targeting and replication efficiency. PLoS pathogens 7:e1002439.
23. Briggs CJ, Ott DE, Coren LV, Oroszlan S, Tozser J. 1999. Comparison of the effect of FK506 and cyclosporin A on virus production in H9 cells chronically and newly infected by HIV-1. Arch Virol 144:2151-60.
24. Freed EO. 2015. HIV-1 assembly, release and maturation. Nature reviews Microbiology 13:484-96.
25. Verhoef K, Koper M, Berkhout B. 1997. Determination of the minimal amount of Tat activity required for human immunodeficiency virus type 1 replication. Virology 237:228-36.
26. Karn J, Stoltzfus CM. 2012. Transcriptional and posttranscriptional regulation of HIV-1 gene expression. Cold Spring Harb Perspect Med 2:a006916.
27. Luban J, Bossolt KL, Franke EK, Kalpana GV, Goff SP. 1993. Human immunodeficiency virus type 1 Gag protein binds to cyclophilins A and B. Cell 73:1067-78.
28. Thali M, Bukovsky A, Kondo E, Rosenwirth B, Walsh CT, Sodroski J, Gottlinger HG. 1994. Functional association of cyclophilin A with HIV-1 virions. Nature 372:363-5.
29. Xu C, Fischer DK, Rankovic S, Li W, Dick RA, Runge B, Zadorozhnyi R, Ahn J, Aiken C, Polenova T, Engelman AN, Ambrose Z, Rousso I, Perilla JR. 2020. Permeability of the HIV-1 capsid to metabolites modulates viral DNA synthesis. PLoS Biol 18:e3001015.
30. Welker R, Hohenberg H, Tessmer U, Huckhagel C, Krausslich HG. 2000. Biochemical and structural analysis of isolated mature cores of human immunodeficiency virus type 1. J Virol 74:1168-77.
31. Wen Y, Feigenson GW, Vogt VM, Dick RA. 2020. Mechanisms of PI(4,5)P2 Enrichment in HIV-1 Viral Membranes. J Mol Biol 432:5343-5364.
32. Dahmane S , Doucet C , Le Gall A , Chamontin C , Dosset P , Murcy F , Fernandez L , Salas D , Rubinstein E , Mougel M , Nollmann M , PE M. 2019. Nanoscale organization of tetraspanins during HIV-1 budding by correlative dSTORM/AFM. Nanoscale 11:6036-6044.
33. McMahon MA, Shen L, Siliciano RF. 2009. New approaches for quantitating the inhibition of HIV-1 replication by antiviral drugs in vitro and in vivo. Curr Opin Infect Dis 22:574-82.
34. Towers GJ, Hatziioannou T, Cowan S, Goff SP, Luban J, Bieniasz PD. 2003. Cyclophilin A modulates the sensitivity of HIV-1 to host restriction factors. Nat Med 9:1138-43.
35. Lalonde MS, Lobritz MA, Ratcliff A, Chamanian M, Athanassiou Z, Tyagi M, Wong J, Robinson JA, Karn J, Varani G, Arts EJ. 2011. Inhibition of both HIV-1 reverse transcription and gene

expression by a cyclic peptide that binds the Tat-transactivating response element (TAR) RNA. PLoS pathogens 7:e1002038.
36. Braaten D, Franke EK, Luban J. 1996. Cyclophilin A is required for an early step in the life cycle of human immunodeficiency virus type 1 before the initiation of reverse transcription. Journal of virology 70:3551-60.
37. Butler SL, Hansen MS, Bushman FD. 2001. A quantitative assay for HIV DNA integration in vivo. Nature medicine 7:631-4.
38. Mousseau G, Clementz MA, Bakeman WN, Nagarsheth N, Cameron M, Shi J, Baran P, Fromentin R, Chomont N, Valente ST. 2012. An analog of the natural steroidal alkaloid cortistatin A potently suppresses Tat-dependent HIV transcription. Cell host & microbe 12:97-108.
39. Jeang KT, Xiao H, Rich EA. 1999. Multifaceted activities of the HIV-1 transactivator of transcription, Tat. J Biol Chem 274:28837-40.
40. Apolloni A, Hooker CW, Mak J, Harrich D. 2003. Human immunodeficiency virus type 1 protease regulation of tat activity is essential for efficient reverse transcription and replication. J Virol 77:9912-21.
41. Bayer P, Kraft M, Ejchart A, Westendorp M, Frank R, Rosch P. 1995. Structural studies of HIV-1 Tat protein. J Mol Biol 247:529-35.
42. Yao XJ, Kobinger G, Dandache S, Rougeau N, Cohen E. 1999. HIV-1 Vpr-chloramphenicol acetyltransferase fusion proteins: sequence requirement for virion incorporation and analysis of antiviral effect. Gene therapy 6:1590-9.
43. Sokolskaja E, Berthoux L, Luban J. 2006. Cyclophilin A and TRIM5alpha independently regulate human immunodeficiency virus type 1 infectivity in human cells. J Virol 80:2855-62.
44. Lahaye X, Satoh T, Gentili M, Cerboni S, Silvin A, Conrad C, Ahmed-Belkacem A, Rodriguez Elisa C, Guichou J-F, Bosquet N, Piel M, Le Grand R, King Megan C, Pawlotsky J-M, Manel N. 2016. Nuclear Envelope Protein SUN2 Promotes Cyclophilin-A-Dependent Steps of HIV Replication. Cell Reports 15:879-892.
45. Fernandez J, Machado AK, Lyonnais S, Chamontin C, Gartner K, Leger T, Henriquet C, Garcia C, Portilho DM, Pugniere M, Chaloin L, Muriaux D, Yamauchi Y, Blaise M, Nisole S, Arhel NJ. 2019. Transportin-1 binds to the HIV-1 capsid via a nuclear localization signal and triggers uncoating. Nat Microbiol 4:1840-1850.
46. Ensoli B, Barillari G, Salahuddin SZ, Gallo RC, Wong-Staal F. 1990. Tat protein of HIV-1 stimulates growth of cells derived from Kaposi's sarcoma lesions of AIDS patients. Nature 345:84-6.
47. Marchio S, Alfano M, Primo L, Gramaglia D, Butini L, Gennero L, De Vivo E, Arap W, Giacca M, Pasqualini R, Bussolino F. 2005. Cell surface-associated Tat modulates HIV-1 infection and spreading through a specific interaction with gp120 viral envelope protein. Blood 105:2802-11.
48. Yu A, Skorupka KA, Pak AJ, Ganser-Pornillos BK, Pornillos O, Voth GA. 2020. TRIM5alpha self-assembly and compartmentalization of the HIV-1 viral capsid. Nat Commun 11:1307.
49. Chapman EH, Kurec AS, Davey FR. 1981. Cell volumes of normal and malignant mononuclear cells. J Clin Pathol 34:1083-90.
50. Zhang J, Tamilarasu N, Hwang S, Garber ME, Huq I, Jones KA, Rana TM. 2000. HIV-1 TAR RNA enhances the interaction between Tat and cyclin T1. J Biol Chem 275:34314-9.
51. Zila V, Margiotta E, Turonova B, Muller TG, Zimmerli CE, Mattei S, Allegretti M, Borner K, Rada J, Muller B, Lusic M, Krausslich HG, Beck M. 2021. Cone-shaped HIV-1 capsids are transported through intact nuclear pores. Cell 184:1032-1046 e18.

52. Francis AC, Melikyan GB. 2018. Single HIV-1 Imaging Reveals Progression of Infection through CA-Dependent Steps of Docking at the Nuclear Pore, Uncoating, and Nuclear Transport. Cell Host Microbe 23:536-548 e6.
53. Vendeville A, Rayne F, Bonhoure A, Bettache N, Montcourrier P, Beaumelle B. 2004. HIV-1 Tat enters T cells using coated pits before translocating from acidified endosomes and eliciting biological responses. Mol Biol Cell 15:2347-60.
54. Ahmed-Belkacem A, Colliandre L, Ahnou N, Nevers Q, Gelin M, Bessin Y, Brillet R, Cala O, Douguet D, Bourguet W, Krimm I, Pawlotsky J-M, Guichou J-F. 2016. Fragment-based discovery of a new family of non-peptidic small-molecule cyclophilin inhibitors with potent antiviral activities. Nature communications 7:12777.
55. Hung M, Niedziela-Majka A, Jin D, Wong M, Leavitt S, Brendza KM, Liu X, Sakowicz R. 2013. Large-scale functional purification of recombinant HIV-1 capsid. PLoS One 8:e58035.
56. Sabers CJ, Martin MM, Brunn GJ, Williams JM, Dumont FJ, Wiederrecht G, Abraham RT. 1995. Isolation of a protein target of the FKBP12-rapamycin complex in mammalian cells. J Biol Chem 270:815-22.
57. Benkirane M, Chun RF, Xiao H, Ogryzko VV, Howard BH, Nakatani Y, Jeang KT. 1998. Activation of integrated provirus requires histone acetyltransferase. p300 and P/CAF are coactivators for HIV-1 Tat. J Biol Chem 273:24898-905.
58. Chatterji U, Lim P, Bobardt MD, Wieland S, Cordek DG, Vuagniaux G, Chisari F, Cameron CE, Targett-Adams P, Parkinson T, Gallay PA. 2010. HCV resistance to cyclosporin A does not correlate with a resistance of the NS5A-cyclophilin A interaction to cyclophilin inhibitors. J Hepatol 53:50-6.
59. Longo PA, Kavran JM, Kim M-S, Leahy DJ. 2013. Transient mammalian cell transfection with polyethylenimine (PEI). Methods in enzymology 529:227-40.
60. Alfaisal J, Machado A, Galais M, Robert-Hebmann V, Arnaune-Pelloquin L, Espert L, Biard-Piechaczyk M. 2019. HIV-1 Vpr inhibits autophagy during the early steps of infection of CD4 T cells. Biol Cell 111:308-318.
61. Paul-Gilloteaux P, Heiligenstein X, Belle M, Domart MC, Larijani B, Collinson L, Raposo G, Salamero J. 2017. eC-CLEM: flexible multidimensional registration software for correlative microscopies. Nat Methods 14:102-103.
62. Mbisa JL, Delviks-Frankenberry KA, Thomas JA, Gorelick RJ, Pathak VK. 2009. Real-time PCR analysis of HIV-1 replication post-entry events. Methods Mol Biol 485:55-72.

## Figure Legends

**Figure 1. Tat interaction with CypA does not require CypA active site and allows the formation of a Tat-CypA-CA tripartite complex**. **A,** HEK 293T cells were transiently transfected with a Gag (left panel) or Tat (right panel) vector. After 36 h, cell lysates were incubated with GST, GST-CypA or GST-CypA-H126Q immobilized on GSH-agarose, before washes and anti-Tat, -p24 or-GST western blots. GST staining using Coomassie blue showed equivalent GST loading. The graph shows the quantification of the amount of Tat or Gag pulled down by H126Q / WT GST-CypA (%). Data are mean ± SEM from n=4-7 experiments. **, $p< 0.01$ (Student's t-test). **B**, Immunoprecipitation of the Tat-CypA-CA complex. HEK 293T cells were transfected with Tat-FLAG, Gag WT, Gag-CA-G89V or empty vector as indicated. After 36 h, Tat-FLAG was immunoprecipitated from cell lysates using an anti-FLAG antibody, before western blots. **C**, GST pull down by GST-Tat. Cells were transfected with Gag WT, Gag-CA-G89V or empty vector as indicated. After 36 h cell lysates were incubated with GST-Tat immobilized on GSH-agarose, before washes and anti-p24 or-GST western blots. GST blots showed similar GST loading.

**Figure 2. Analysis of the CA-CypA-Tat complex by size exclusion chromatography.** Indicated recombinant protein mixtures (CA, CypA, Tat or the indicated combination) were incubated for 30 min at RT then loaded on a Superdex 200 Increase column. **A**, protein elution profile monitored using $ABS_{280}$. **B**, The elution volume corresponding to the maximum $ABS_{280}$ of the first peak (CA peak~ 14 ml) is shown. Means ± SEM of n= 3 injections. **, $p<0.01$ (One Way ANOVA). **C**, fractions corresponding to the capsid (~14 ml), CypA (~17ml) and Tat (19-20 ml) peaks were analyzed by western blot. CypA* is CypA-H126Q.

**Figure 3. Analysis of the interactions involved in the assembly of the Tat-CypA-CA complex. A,** analysis by MST. CypA was fluorescently labeled and its interaction with increasing concentrations of Tat or CA was tested. When indicated by (CypA+CA) or (CypA+Tat), fluorescent CypA (50 nM) was first mixed with a saturating concentration of CA (20 µM) or Tat (1 µM) before adding escalating concentrations of the third partner. **B,** analysis by SPR. For the top panels, Tat was immobilized on the Biacore chip before applying the indicating partner using escalating concentrations. CypA (upper left panel) or premixed CypA+CA (upper right panel) were applied at 0.37 / 0.75/ 1.5 / 3 / 6 µM. When indicated (Tat+CypA on chip), CypA (4 µM) was applied to immobilized Tat before applying CA (0.37 / 0.75/ 1.5 / 3 / 6 µM) to monitor CA binding to CypA presented by Tat. For the bottom right panel, CA was immobilized on the chip, before applying CypA at 0.37-6 µM. Arrows indicate injections. **C**, Graphical abstract of the affinities involved in the assembly of the Tat-CypA-CA complex as observed using MST and SPR.

**Figure 4. HIV-1 Tat is encapsidated in a CypA-dependent manner. A,** Transfected cells. HEK cells were transfected with pNL4.3, either WT, Tat-W11Y, Tat-C31S or CA-G89V as indicated. After 48 h, viruses were purified from the supernatant by ultracentrifugation through a sucrose cushion, before analysis by western blots. Two different antibodies were used for Tat, one that recognizes the N-ter of the protein (res1-9) and a second whose epitope is conformational (Conf). Tat-W11Y was not recognized by the antibody against the N-ter of the protein. Overexposed gels only enabled Tat detection in CA-G89V virions, that are devoid of CypA. The graph shows the amount of Tat (N-ter)/p24 for the four different viruses (n=2, mean ± SEM). **B,** Infected cells. $HIV_{NL4.3}$ WT or CA-G89V was used to infect Jurkat-CD4-CCR5 cells and infection was allowed to proceed for 9 days adding fresh cells every 3 days before harvesting virions for analysis. When indicated 2 µM CSA was added to cells to prevent CypA encapsidation. The graph shows the amount of Tat (N-ter) / p24 for the three different viruses (n=2, mean ± SEM). **C,** Capsid cores from WT, CSA or CA-G89V viruses were purified following Triton X-100 treatment to solubilize the viral envelope and both purified viruses and capsid cores were analyzed by western blots against the indicated proteins. **D,** purified WT or CA-G89V virions were coated on coverslips and labelled using antibodies against p24 (red) and Tat (green) before AFM and TIRF imaging. Images were aligned using Ec-CLEM. Viruses were identified as AFM spots >100 nm. AFM-identified virions are circled in red, green or yellow if they are positive for CA, Tat or both, respectively. Scale bars are 10 µm and 2 µm for fluorescence and AFM images, respectively. Representative images are shown. The graph corresponds to the percentage of viruses ($AFM^+$ and $CA^+$) containing Tat for WT and CA-G89V virions (n=3 from entirely independent experiments; mean ± SEM; Student's t-test ***, $p<0.001$).

**Figure 5. Encapsidated HIV-1 Tat is delivered to the cytosol and is required for efficient HIV infection**

**A**, Cytosolic delivery assay. Human CD4 primary T-cells were transfected with LTR-firefly luciferase and TK-renilla luciferase (control vector). After 18 h, cells were infected with the pseudotyped $HIV_{NL4.3}$, either WT or CA-G89V or prepared in the presence of 2 µM CSA. Infections were performed in the presence of 20 µM AZT to inhibit Tat neosynthesis. Cells were lysed 24 h post-infection to assay luciferase activities. The graph shows the Firefly/Renilla activity ratio (mean ± SEM; n=3). Graphs showing firefly and renilla activities are presented in Fig. S3. One Way ANOVA compared to WT virus ***, $p<0.001$; ****, $p<0.0001$. **B, C, D, E,** single-round infections. Jurkat T-cells (**B, C**) and human primary CD4 T-cells (**D, E**) were infected with the indicated amount (ng p24) of VSV-G pseudotyped $HIV_{NL4.3}$ viruses. No CSA was added, it was used during viral production by HEK cells only. After 36h, cells were stained for p24 before FACS analysis (**B,D**) to determine the efficiency of infection (%), and virus concentration in the cell medium was assayed using p24 ELISA (**C, E**). Data are mean ± SEM from n=3 independent experiments. Error bars are within the symbol size.

**Figure 6. Encapsidated Tat and/or CypA increase reverse transcription and strongly stimulate transcription**

**A**, Quantification of early and late RT products. Jurkat T-cells were infected with $HIV_{NL4.3}$, either WT or CA-G89V or prepared in the presence of 2 µM CSA. Cells were harvested 6 h after infection for DNA extraction and qPCR. **B**, Quantification of integrated provirus. Cell DNA was extracted 24h or 34h after infection before Alu-PCR and late RT-PCR to quantify viral DNA. **C,** q-RT-PCR of viral RNA. Cell RNA was extracted 24h or 34h after infection and reversed transcribed to cDNA for qPCR. Transcript quantifications were normalized using integrated viral-DNA amount. Data are presented as % of WT virus for each time point, and are means ± SEM of 3 independent experiments, each with n=3. Two Way ANOVA, ****, $p<0.0001$.

**Figure 7. Encapsidated Tat regulates transcription, reverse transcription, infection and viral production**

**A**, ΔTat ΔEnv pNL4.3 was cotransfected in HEK293T cells with VSV-G to pseudotype virions and a vector coding for Tat WT, C22S, Y47H or 22S-47H as indicated. Tat mutants were cotransfected with WT Tat (ratio 1 WT/ 2 mutant) to insure significant viral production by Tat-C22S that is transcriptionally inactive. Viruses were purified for biochemical analysis by western blot. **B**, Quantification of early and late RT products. Tat-complemented ΔTat pseudotyped viruses were used to infect Jurkat T-cells. Cells were harvested 6h after infection for DNA extraction and qPCR. **C,** Quantification of integrated provirus. Cell DNA was extracted 24h after infection before Alu-PCR and late RT-PCR to quantify viral DNA. **D**, q-RT-PCR of viral RNA. Cell RNA was extracted 24h after infection and reversed transcribed to cDNA for qPCR. Transcript quantification was normalized using integrated viral-DNA amount. Data are presented as % of WT virus, and are means ± SEM of 3 independent experiments, each with n=3. **E** and **F,** Tat-complemented viruses were used to infect Jurkat cells in single-round infection assays. After 24h, cells were stained for p24 before FACS analysis (**E**) to determine the efficiency of infection (%), and virus concentration in the cell medium was assayed using p24 ELISA (**F**). Data are mean ± SEM (n=3-5). Results were normalized for Tat encapsidation efficiency. One- (**C**,**D,E,F**) or Two- Way (**B**) ANOVA, *, $p<0.05$; **, $p<0.01$; ***, $p<0.001$; ****, $p<0.0001$.

**Figure 8. Complementation of CA-G89V viruses with Tat-Vpr indicates that encapsidation of transcriptionally-active Tat strongly stimulates infection**

CA-G89V pNL4.3 was cotransfected in HEK293T cells with a vector coding for the indicated Vpr chimera, and VSV-G to pseudotype viruses. **A,** biochemical analysis by Western blots. Anti-Vpr detects the endogenous viral Vpr at 12.5 kDa, Tat-Vpr at 22 kDa and CypA-Vpr at 27 kDa. **B** and **C,** CA-G89V viruses with Vpr chimera were used to infect Jurkat cells in single-round infection assays before intracellular p24 staining (FACS analysis, **B**) and p24 ELISA to assay viral production in the medium (**C**). Data are means ± SEM (n=2-3) of a typical experiment that was repeated twice. One Way ANOVA, *, <0.05; **, $p<0.01$; ***, $p<0.001$; ****, $p<0.0001$.

# Figure 1

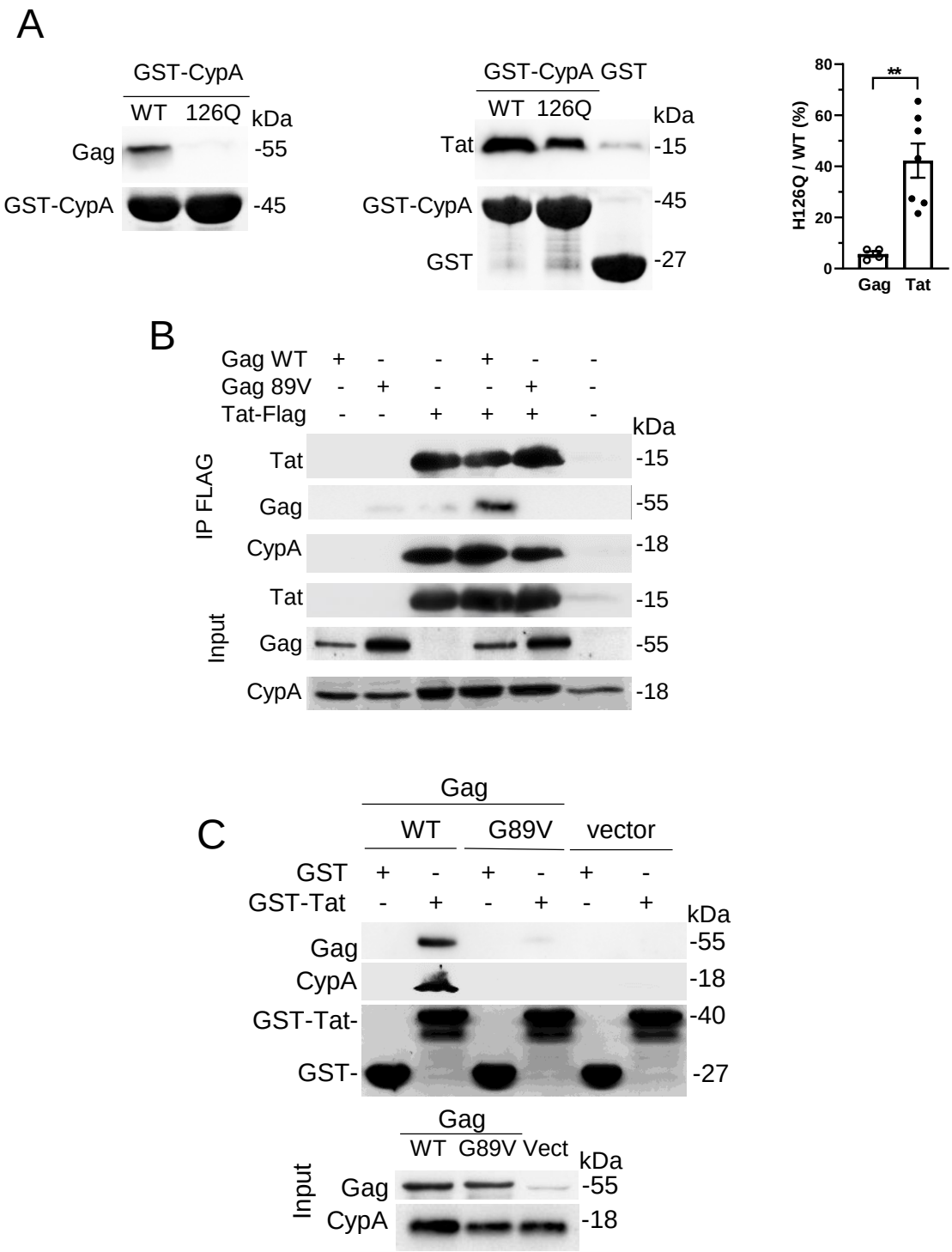
A
GST-CypA
WT 126Q kDa
Gag -55
GST-CypA -45
GST-CypA GST
WT 126Q kDa
Tat -15
GST-CypA -45
GST -27
H126Q / WT (%)
80
60
40
20
0
**
Gag Tat
B
Gag WT + - - + - -
Gag 89V - + - - + -
Tat-Flag - - + + + -
kDa
IP FLAG
Tat -15
Gag -55
CypA -18
Input
Tat -15
Gag -55
CypA -18
C
Gag
WT G89V vector
GST + - + - + -
GST-Tat - + - + - +
kDa
Gag -55
CypA -18
GST-Tat- -40
GST- -27
Gag
WT G89V Vect
Input
kDa
Gag -55
CypA -18

Figure 2

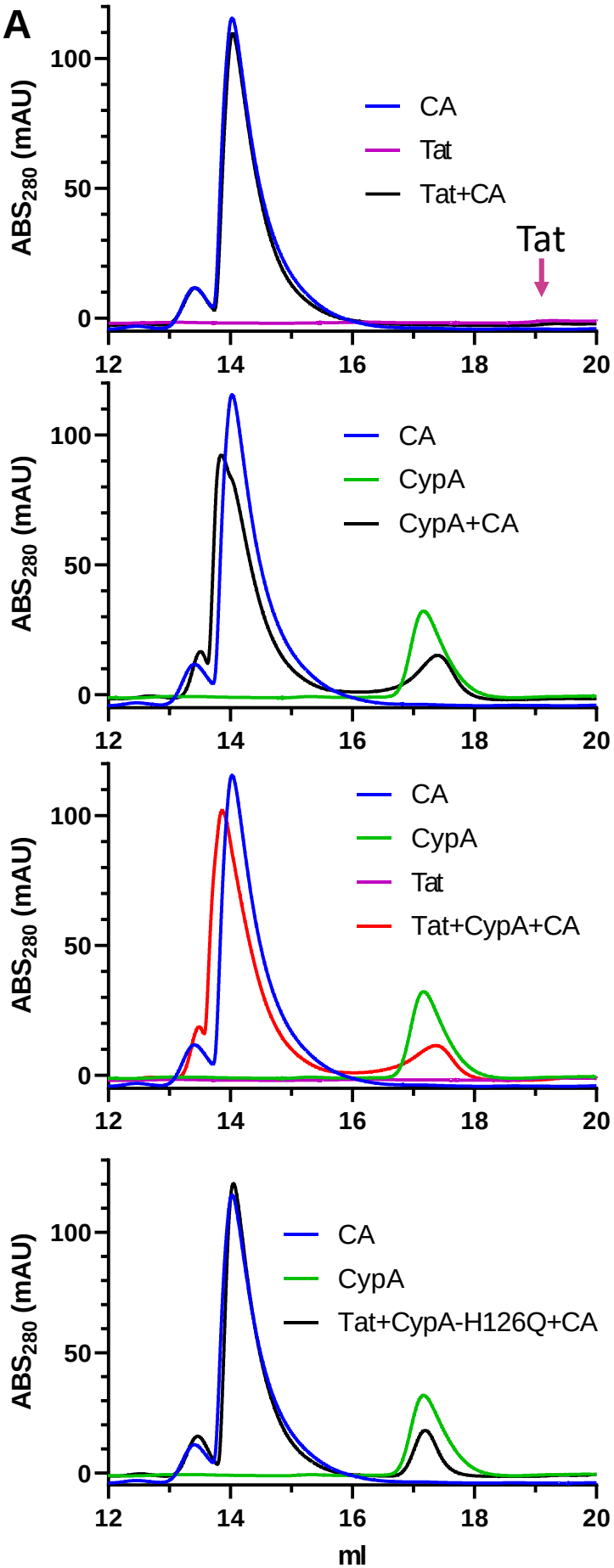
A
ABS280 (mAU)
100
50
0
12
14
16
18
20
CA
Tat
Tat+CA
Tat
CA
CypA
CypA+CA
CA
CypA
Tat
Tat+CypA+CA
CA
CypA
Tat+CypA-H126Q+CA
ml

Figure 2

**B**

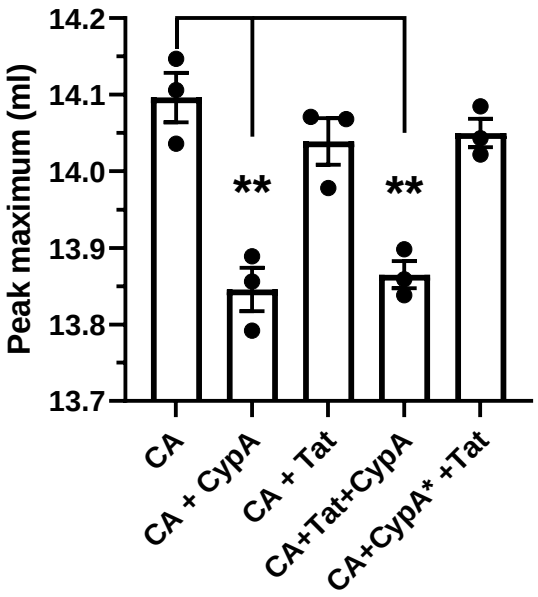
Peak maximum (ml)
14.2
14.1
14.0
13.9
13.8
13.7
**
**
CA
CA + CypA
CA + Tat
CA+Tat+CypA
CA+CypA* +Tat

**C**

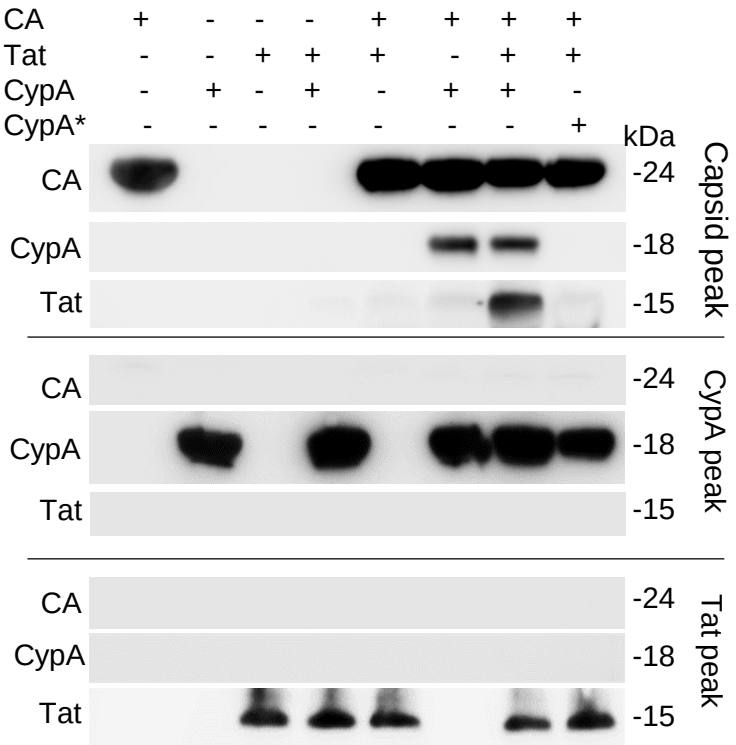
CA + - - - + + + +
Tat - - + + + - + +
CypA - + - + - + + -
CypA* - - - - - - - +
kDa
CA
CypA
Tat
-24
-18
-15
Capsid peak
CA
CypA
Tat
-24
-18
-15
CypA peak
CA
CypA
Tat
-24
-18
-15
Tat peak

Figure 3

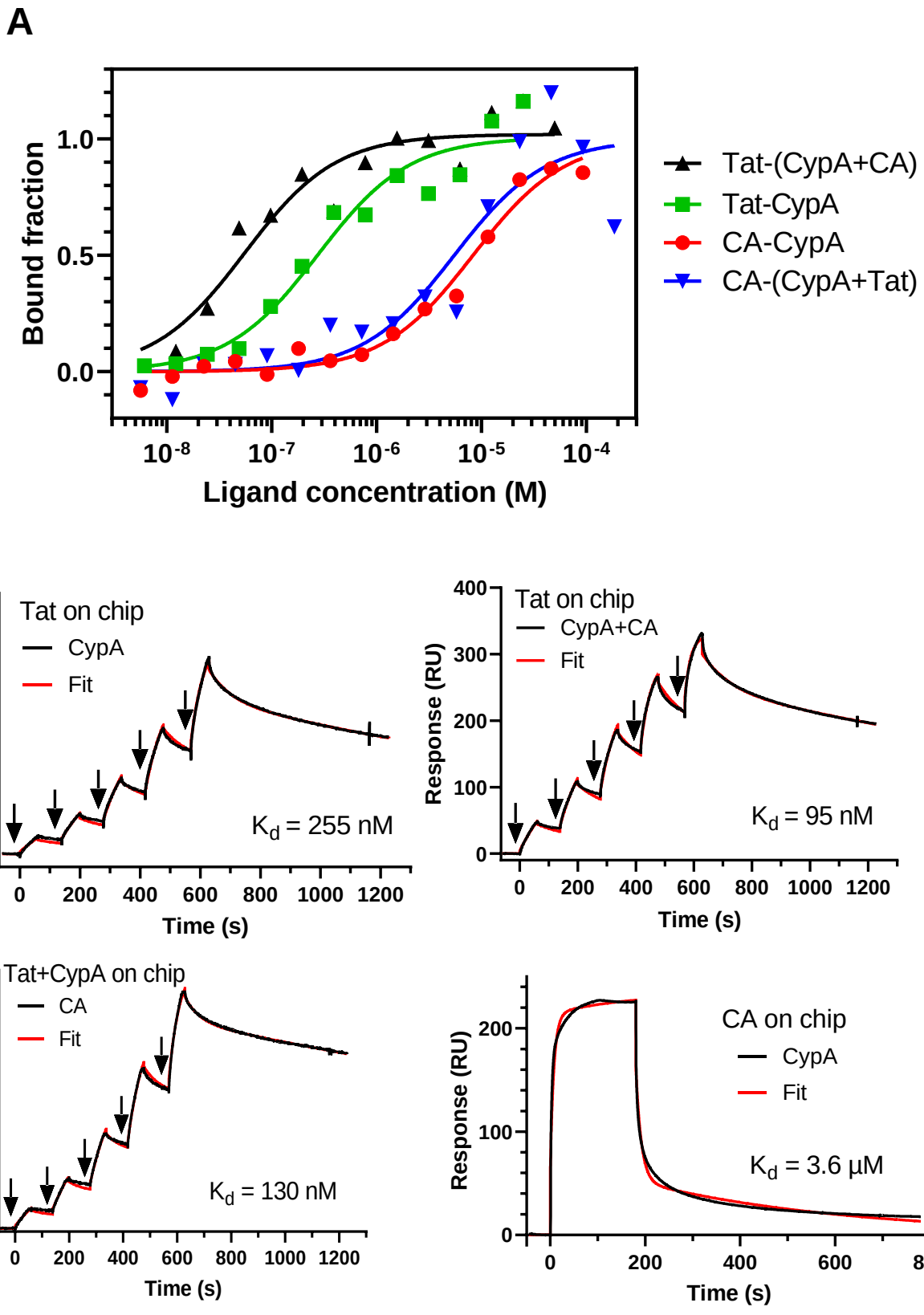
A
Bound fraction
1.0
0.5
0.0
10-8
10-7
10-6
10-5
10-4
Ligand concentration (M)
Tat-(CypA+CA)
Tat-CypA
CA-CypA
CA-(CypA+Tat)
B
Tat on chip
CypA
Fit
Kd = 255 nM
Response (RU)
Time (s)
Tat on chip
CypA+CA
Fit
Kd = 95 nM
Tat+CypA on chip
CA
Fit
Kd = 130 nM
CA on chip
CypA
Fit
Kd = 3.6 µM

# Figure 3

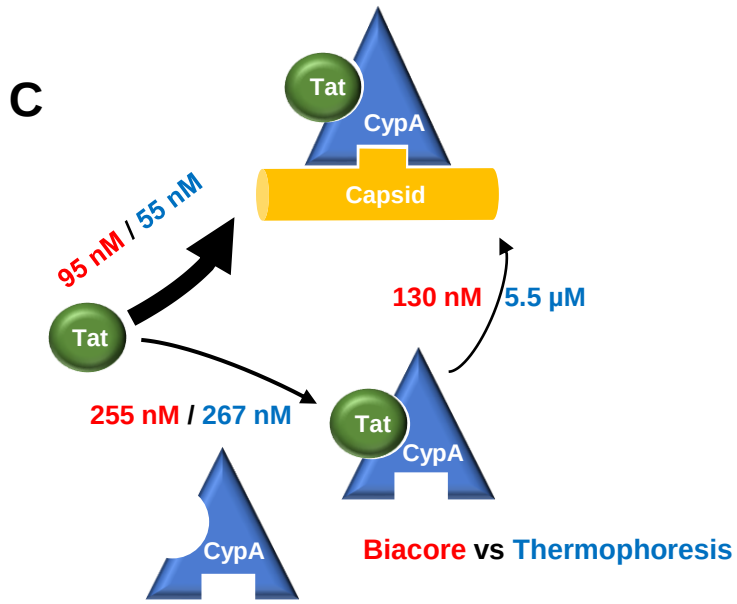
C
Tat
CypA
Capsid
95 nM / 55 nM
Tat
130 nM
5.5 µM
255 nM / 267 nM
Tat
CypA
CypA
Biacore vs Thermophoresis

# Figure 4

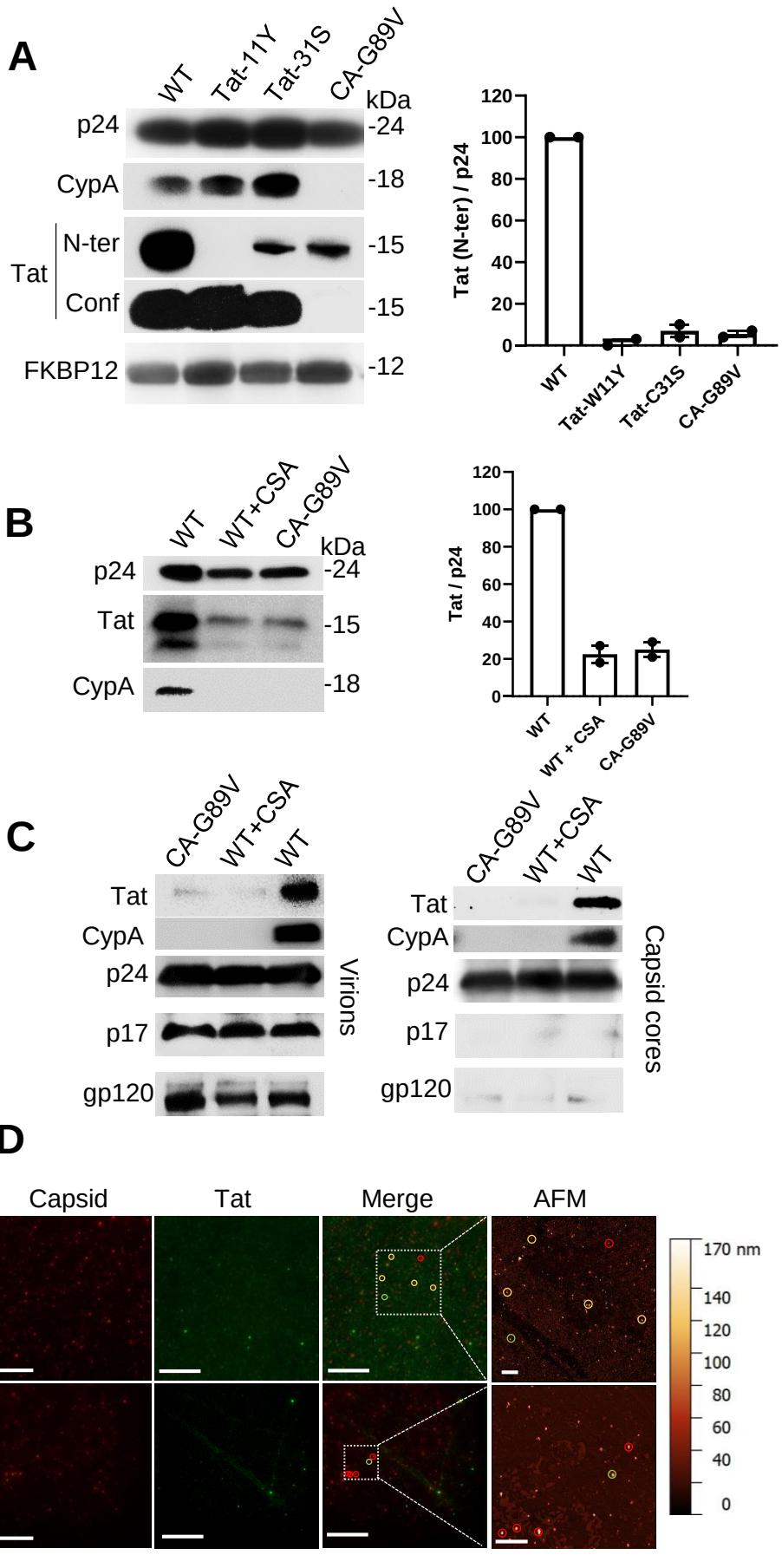
A
WT
Tat-11Y
Tat-31S
CA-G89V
kDa
p24
-24
CypA
-18
Tat
N-ter
-15
Conf
-15
FKBP12
-12
Tat (N-ter) / p24
120
100
80
60
40
20
0
WT
Tat-W11Y
Tat-C31S
CA-G89V
B
WT
WT+CSA
CA-G89V
kDa
p24
-24
Tat
-15
CypA
-18
Tat / p24
120
100
80
60
40
20
0
WT
WT + CSA
CA-G89V
C
CA-G89V
WT+CSA
WT
Tat
CypA
p24
p17
gp120
Virions
CA-G89V
WT+CSA
WT
Tat
CypA
p24
p17
gp120
Capsid cores
D
Capsid
Tat
Merge
AFM
WT
CA-G89V
170 nm
140
120
100
80
60
40
0
Tat-containing viruses (%)
100
50
0
***
WT G89V

Figure 5

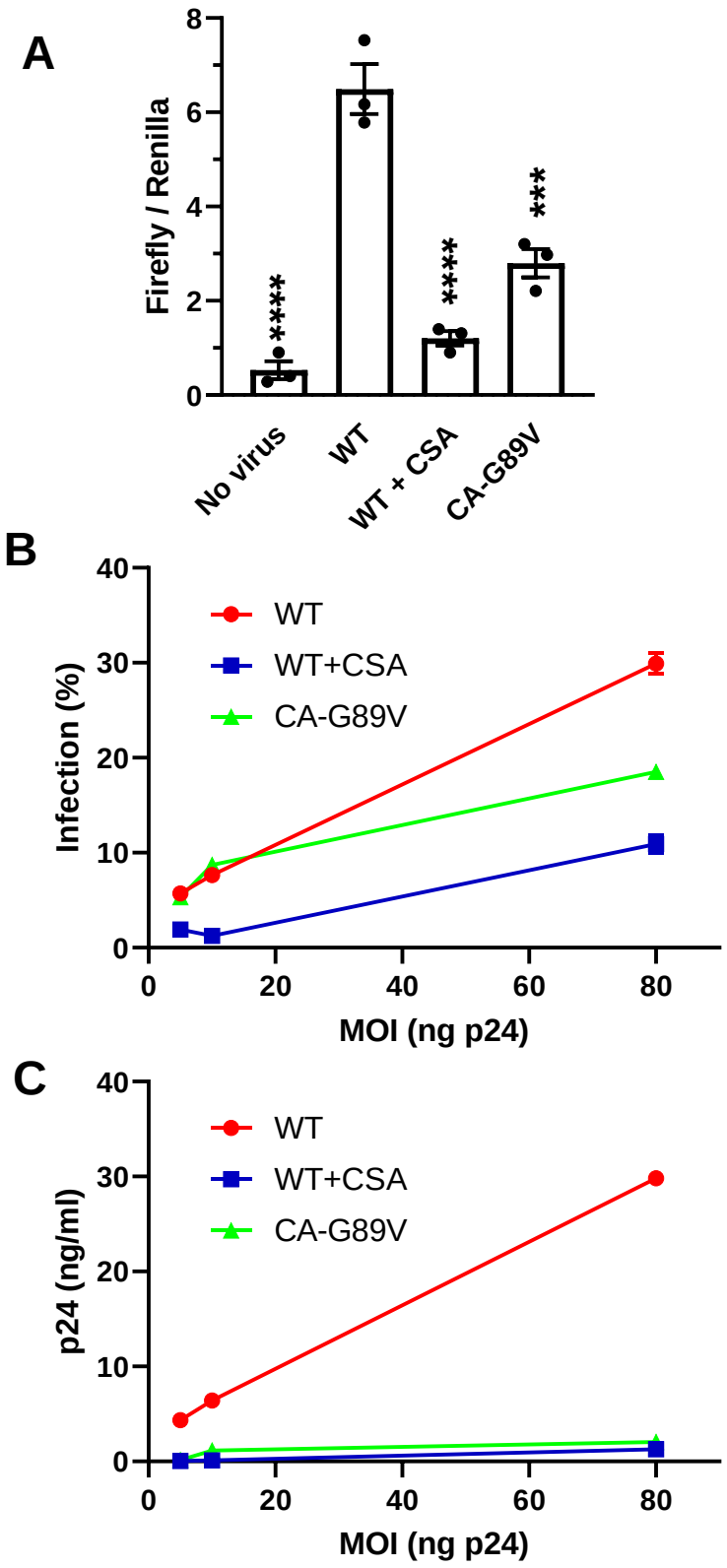
A
Firefly / Renilla
8
6
4
2
0
****
****
***
No virus
WT
WT + CSA
CA-G89V
B
Infection (%)
40
30
20
10
0
WT
WT+CSA
CA-G89V
0
20
40
60
80
MOI (ng p24)
C
p24 (ng/ml)
40
30
20
10
0
WT
WT+CSA
CA-G89V
0
20
40
60
80
MOI (ng p24)

Figure 5

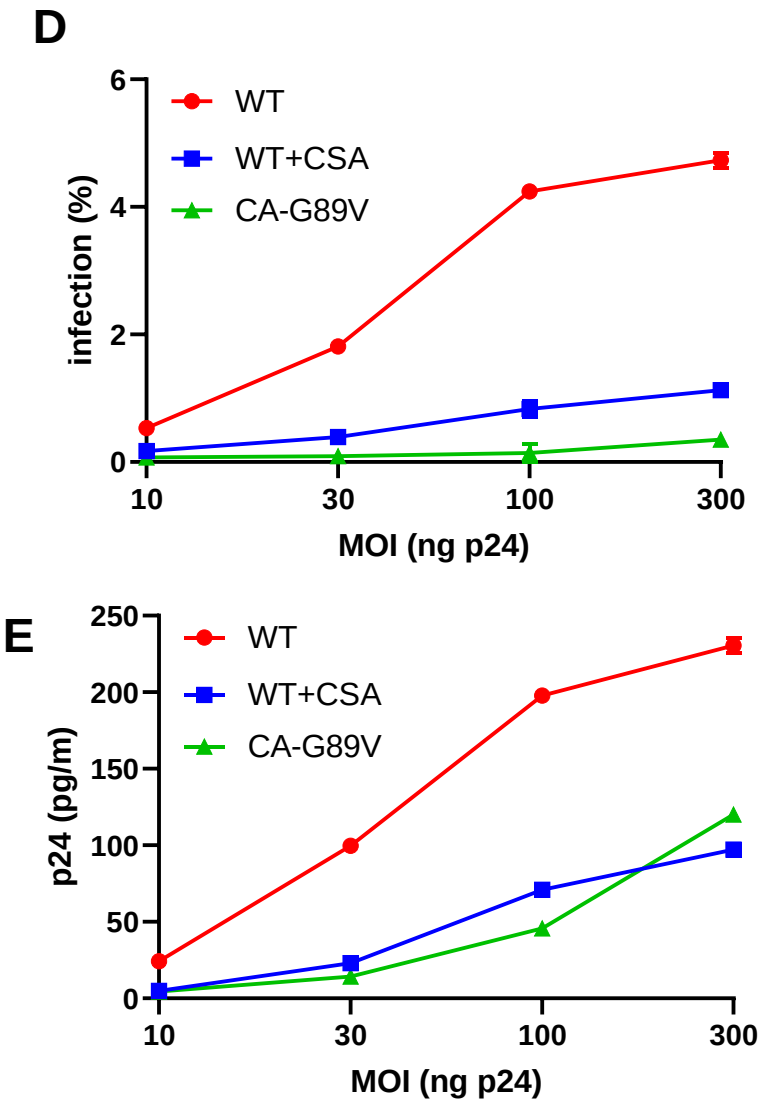
D
6
4
2
0
infection (%)
WT
WT+CSA
CA-G89V
10
30
100
300
MOI (ng p24)
E
250
200
150
100
50
0
p24 (pg/m)
WT
WT+CSA
CA-G89V
10
30
100
300
MOI (ng p24)

Figure 6

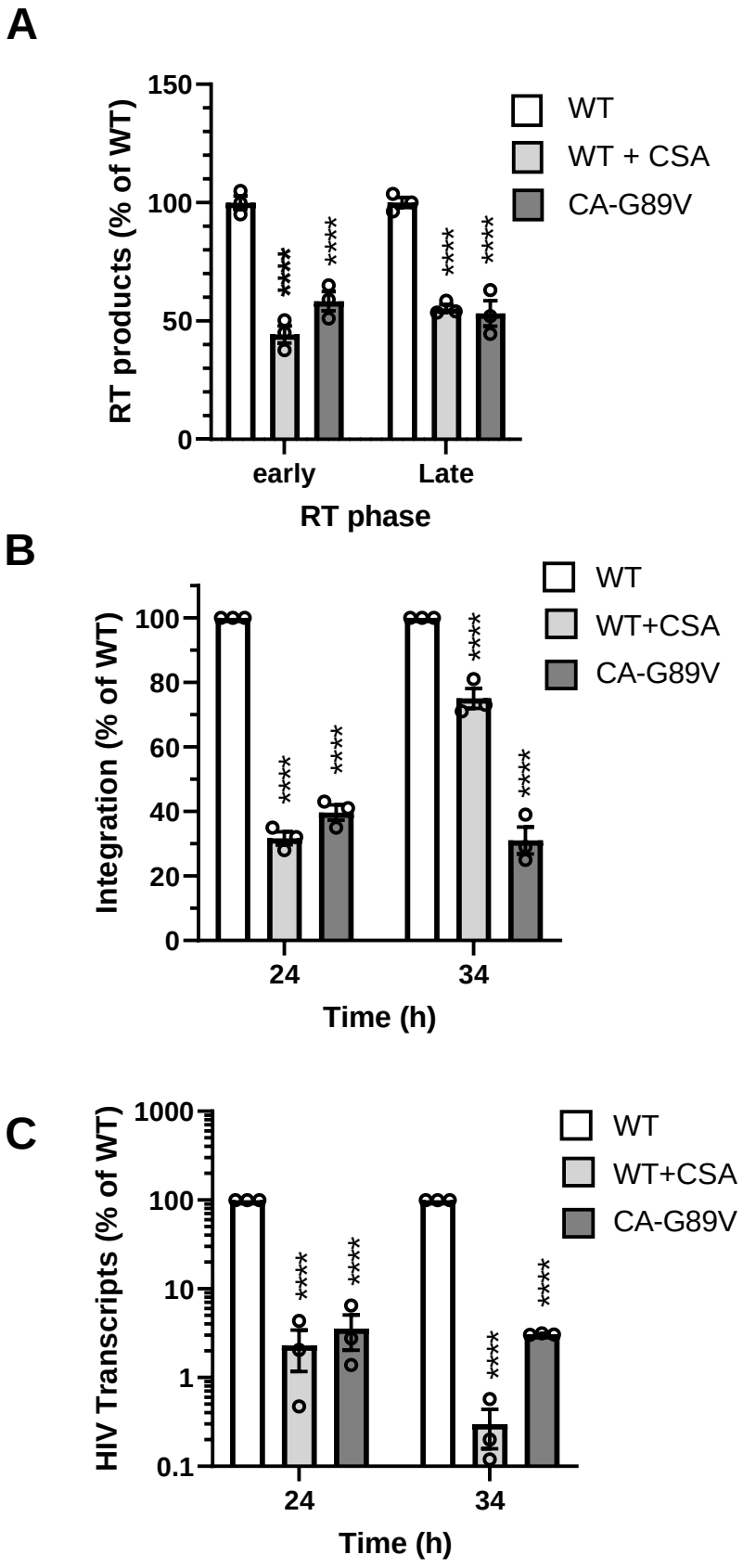
A
RT products (% of WT)
150
100
50
0
WT
WT + CSA
CA-G89V
****
****
****
****
early
Late
RT phase
B
Integration (% of WT)
100
80
60
40
20
0
WT
WT+CSA
CA-G89V
****
****
****
****
24
34
Time (h)
C
HIV Transcripts (% of WT)
1000
100
10
1
0.1
WT
WT+CSA
CA-G89V
****
****
****
****
24
34
Time (h)

# Figure 7

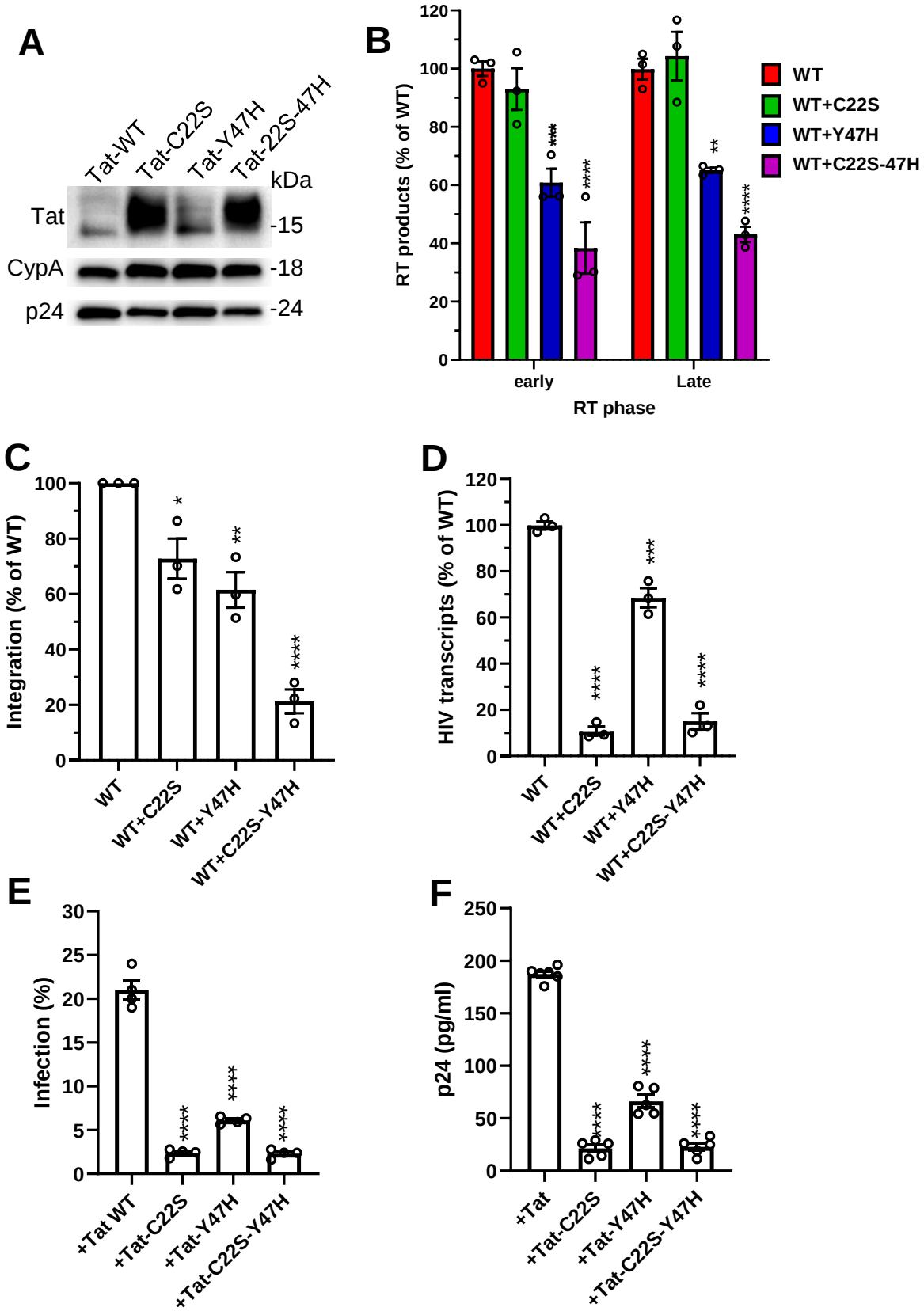
A
Tat-WT
Tat-C22S
Tat-Y47H
Tat-22S-47H
kDa
Tat
-15
CypA
-18
p24
-24
B
RT products (% of WT)
120
100
80
60
40
20
0
early
Late
RT phase
WT
WT+C22S
WT+Y47H
WT+C22S-47H
C
Integration (% of WT)
WT
WT+C22S
WT+Y47H
WT+C22S-Y47H
D
HIV transcripts (% of WT)
WT
WT+C22S
WT+Y47H
WT+C22S-Y47H
E
Infection (%)
+Tat WT
+Tat-C22S
+Tat-Y47H
+Tat-C22S-Y47H
F
p24 (pg/ml)
+Tat
+Tat-C22S
+Tat-Y47H
+Tat-C22S-Y47H

Figure 8

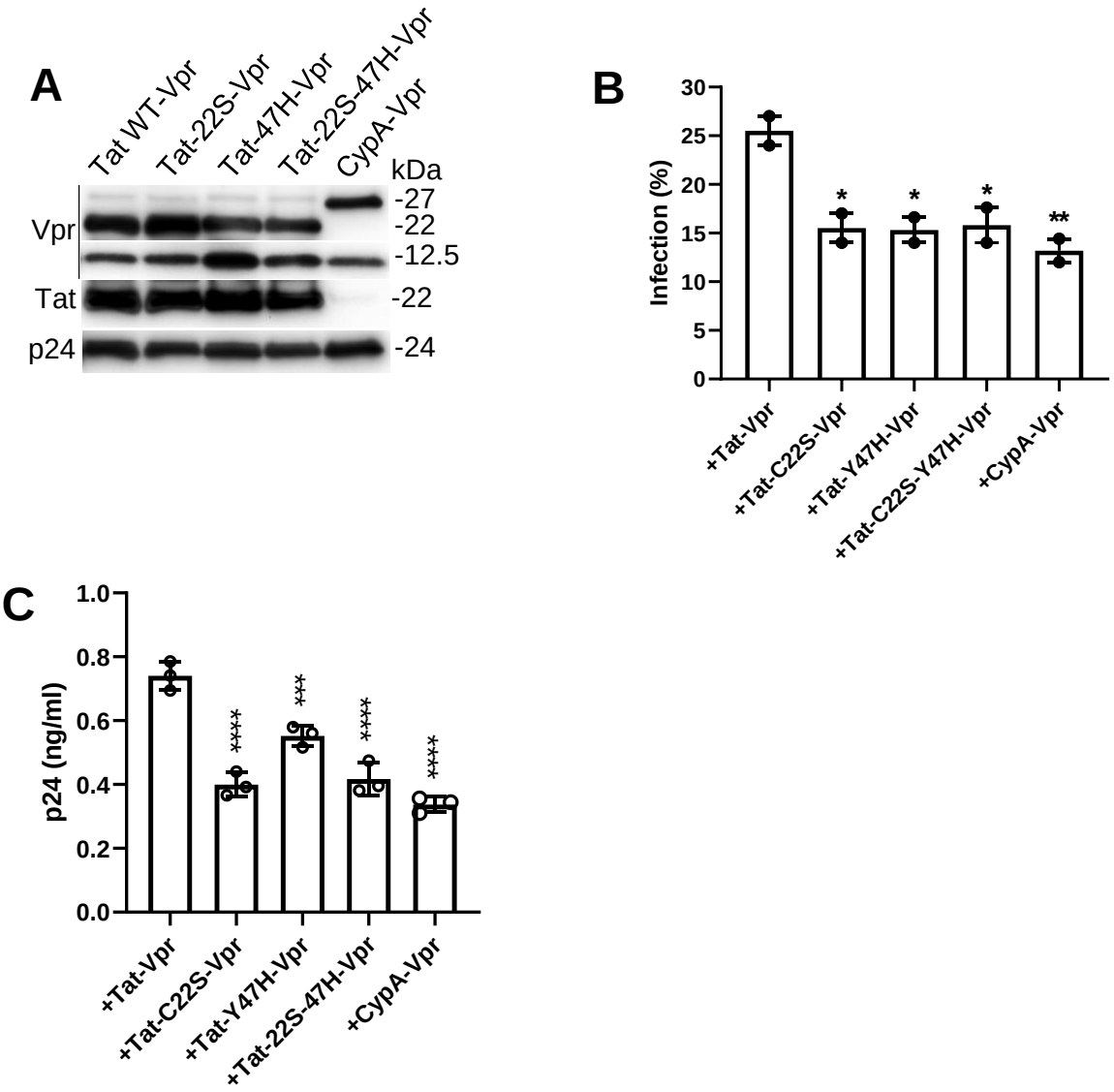
A
Tat WT-Vpr
Tat-22S-Vpr
Tat-47H-Vpr
Tat-22S-47H-Vpr
CypA-Vpr
kDa
Vpr
Tat
p24
-27
-22
-12.5
-22
-24
B
Infection (%)
30
25
20
15
10
5
0
*
*
*
**
+Tat-Vpr
+Tat-C22S-Vpr
+Tat-Y47H-Vpr
+Tat-C22S-Y47H-Vpr
+CypA-Vpr
C
p24 (ng/ml)
1.0
0.8
0.6
0.4
0.2
0.0
****
***
****
****
+Tat-Vpr
+Tat-C22S-Vpr
+Tat-Y47H-Vpr
+Tat-22S-47H-Vpr
+CypA-Vpr

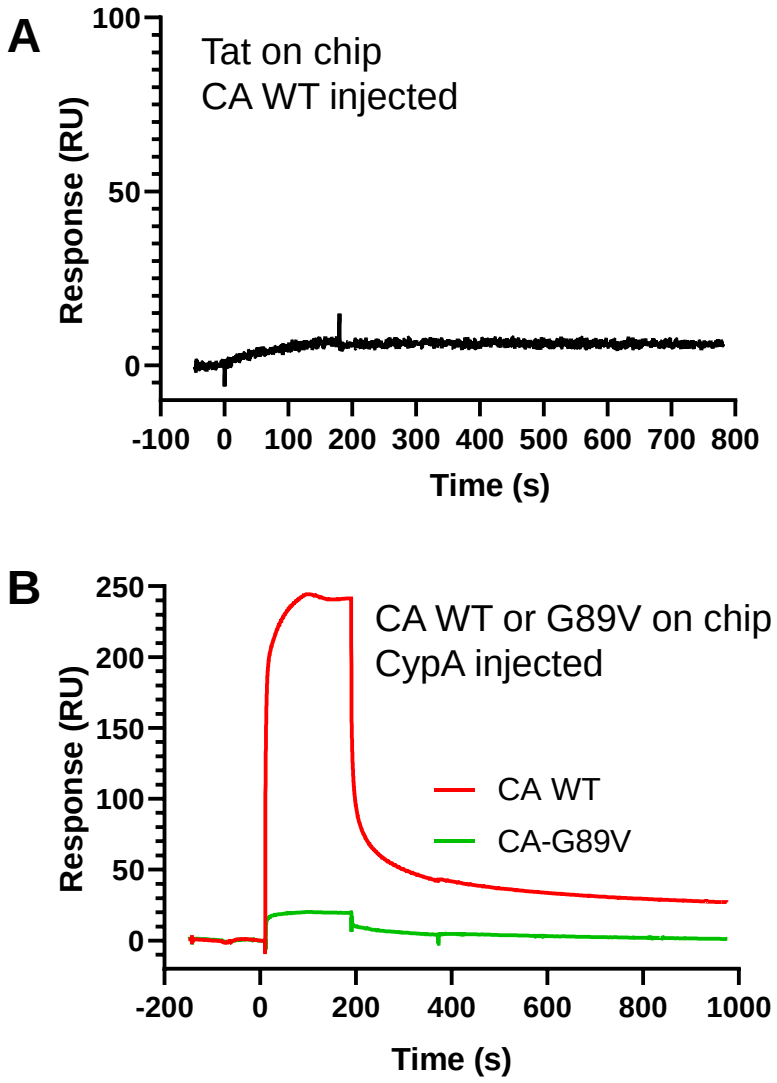


**Figure S1.** SPR analysis. A, Tat does not directly interact with CA. Tat was immobilized on a chip before applying 2 µM CA WT. B, CypA binds to CA WT but not CA-G89V. Capsid proteins were immobilized on a chip before applying 15 µM CypA.

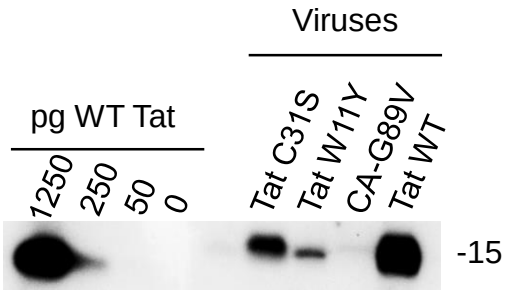


**Figure S2.** Semiquantitative blot of purified viruses. Proteins from WT or mutant viruses and recombinant Tat standards (101 residues) were separated on 16 % Tricine gels before anti-Tat western blot.

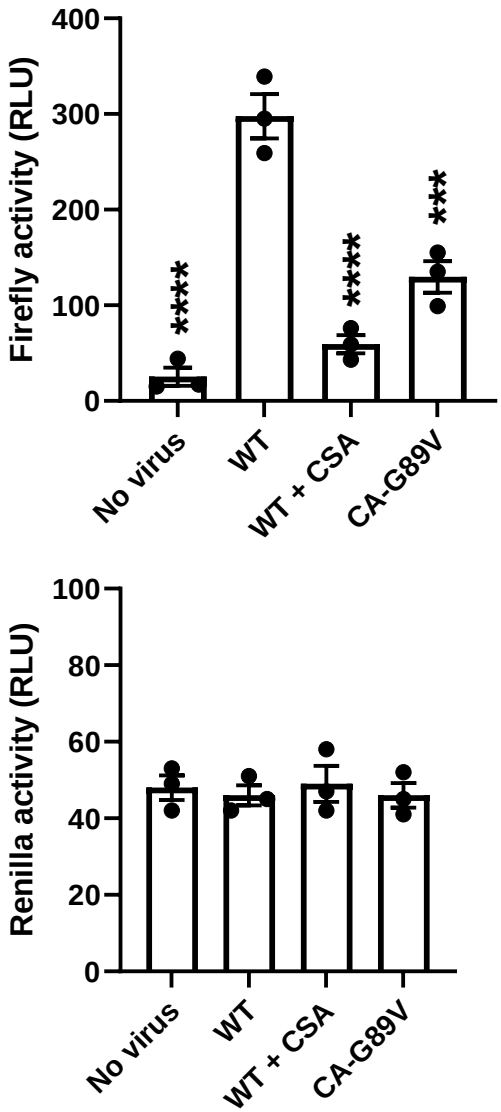


**Figure S3.** Cytosolic delivery assay. Human CD4 primary T-cells were transfected with LTR-firefly luciferase and TK-renilla luciferase (control vector). After 18 h, cells were infected with pseudotyped $HIV_{NL4.3}$, either WT or CA-G89V or prepared in the presence of 2 µM CSA. Infections were performed in the presence of 20 µM AZT to inhibit Tat neosynthesis. Cells were lysed 24 h post-infection to assay luciferase activities. The graphs show the luciferase activities (mean ± SEM; n=3). One Way ANOVA compared to WT virus; ***, $p<0.001$; ****, $p<0.0001$. The firefly/renilla graph is shown in Fig.5A.

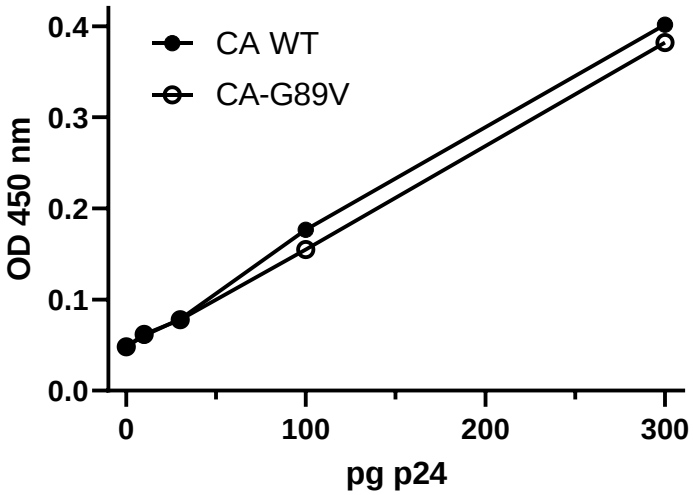


**Figure S4.** WT and G89V capsids are similarly detected using p24 ELISA. HIV-1 capsid proteins were produced and purified from *E. coli* as described in methods and ELISA was performed as recommended by the manufacturer. Means ± SEM (n=2). Error bars are within the symbol size.

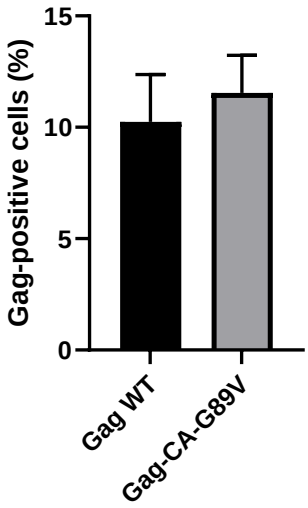


**Figure S5.** Gag-WT and Gag-CA-G89V capsids are similarly detected byKc57-FITC and FACS analysis. Jurkat cells were transfected with Gag-WT or Gag-CA-G89V as indicated. Cells were washed then fixed and permeabilized before staining with Kc57-FITC and analysis by FACS. Means ± SEM (n=2).

# Schatz et al. Sources of antibodies

| Antigen | Ab species | Label | source | reference |
|---|---|---|---|---|
| Tat | Mouse monoclonal | | SantaCruz Biotechnology (NB the epitope is in N-ter) | sc65912 |
| Tat | Rabbit | | E. Loret | home made |
| Tat | Mouse monoclonal | | E. Loret (NB conformational epitope) | 7G12 |
| CypA | Rabbit | | SantaCruz Biotechnology | sc133494 |
| CypA | Goat | | R/D Systems | AF3589 |
| HIV p17 (MA) | Human Monoclonal | | NIBSC (UK) | ADP3057 |
| HIV p24 (CA) | Goat | | BioRad | 4999-9007 |
| HIV p24 (CA) | Mouse monoclonal | | AIDS Research and Reference Reagent Program | 183-H12-5C |
| HIV p24 (CA) | Mouse monoclonal | RD1 | Beckman Coulter | Kc57-RD1 |
| HIV gp160 | Goat | | HIV reagent program | 188 |
| FKBP12 | Rabbit | | Pierce | PA1-026A |
| Mouse IgG | Goat | HRP | Jackson Immunoresearch | 115-035-146 |
| Rabbit IgG | Goat | HRP | Jackson Immunoresearch | 111-035-144 |
| Rabbit IgG | Swine | FITC | Nordic | F0205 |
| Goat IgG | Rabbit | HRP | Sigma | A-5420 |
| Goat IgG | Donkey | AlexaFluor647 | Invitrogen | A21447 |

Antibodies are polyclonal except when otherwise indicated.